

Medium effects on the electromagnetic form factors of ρ meson

Parada T. P. Hutaauruk^{1,2,*}, Terry Mart^{2,†} and Kazuo Tsushima^{3,‡}

¹*Department of Physics, Pukyong National University (PKNU), Busan 48513, Korea*

²*Departemen Fisika, FMIPA, Universitas Indonesia, Depok 16424, Indonesia*

³*Laboratório de Física Teórica e Computacional-LFTC,
Programa de Pósgraduação em Astrofísica e Física Computacional,
Universidade Cidade de São Paulo, 01506-000 São Paulo, SP, Brazil
(Dated: August 29, 2025)*

The dynamics of partons inside the light ρ meson is found to be essential for its properties and internal structure, both in free space and in the nuclear medium. In this paper, we systematically investigate the in-medium structure changes of ρ^+ mesons within the covariant Nambu-Jona-Lasinio (NJL) model, utilizing the Schwinger proper-time regularization scheme. We solve the Bethe-Salpeter equations to guarantee the bound meson-state condition. At the quark level, the nuclear medium effects are also derived within the same NJL model to maintain a consistent approach with the in-medium ρ^+ meson electromagnetic form factors. To this end, we analyze the spacelike electromagnetic form factors of the ρ^+ meson in free space and in a nuclear medium. We find that the charge radius and quadrupole moment of the ρ^+ meson increase with increasing nuclear matter density, while the magnetic moment decreases, in agreement with the existing previous theoretical predictions. The enhancement of the ρ^+ meson charge radius at normal density relative to that in free space is about 11% (0.08 fm), while the reduction of ρ^+ meson magnetic moment is about 8% ($0.20 \mu_N$). Our predictions for the charge radius, magnetic moment, and quadrupole moment of the ρ^+ meson in both free space and nuclear medium, remain challenging to be verified experimentally.

Keywords: Nambu-Jona-Lasinio model, Schwinger proper-time regularization scheme, charge radius, vector meson, magnetic moment, quadrupole moment, electromagnetic form factors

I. INTRODUCTION

Quantum Chromodynamics (QCD) is widely believed to be an underlying theory of strong interaction of the Standard Model (SM) [1]. The nonperturbative QCD at the low-energy scale depends sensitively on the strong running coupling constant $\alpha_s(Q^2)$. Recent interest in the running coupling has increased in focusing on its behavior in relation to gluon saturation phenomena at small quark longitudinal momentum x (Bjorken- x) and the low negative values of the squared four-momentum transfer ($q^2 \equiv -Q^2 < 0$), where nonlinear QCD effects become significant [2, 3]. Rather different from the perturbative QCD aspects, which are relatively well understood and more straightforward to apply, the nonperturbative QCD, which has the properties of confinement and spontaneous or dynamical chiral symmetry breaking (SCSB or DCSB), is still not fully understood until now. These features of nonperturbative QCD are expected to be better understood by studying the internal structure of hadrons, such as the parton distribution functions (PDFs), electromagnetic form factors (EMFFs), parton distribution amplitudes (PDAs), transverse momentum dependent parton distribution functions (TMD-PDFs), gravitational form factors (GFFs), and generalized parton distribution functions (GPDs), in free space as well as in a nuclear medium. As is well known, hadrons can be described effectively as either three valence dressed quarks for baryons or a dressed valence quark-antiquark pair for mesons, with their internal quark dynamics governed by the strong interaction of QCD.

In the 50 years of the existence of QCD [4], much impressive progress has been made in studying the free space properties of the hadrons to better understand QCD [5–16]. The information on the internal structure of hadrons has been obtained through the PDFs [17, 18], EMFFs [13], PDAs [19–21], TMDs [22, 23], GFFs [24, 25], and GPDs [26]. These physical properties have been extensively studied, mostly in free space. In addition to the studies in free space, the features of QCD can also be explored by investigating hadrons in a medium, e.g., through their structure functions in nuclei or nuclear matter [27]. The European Muon Collaboration (EMC) experiment provided clear evidence that the hadron unpolarized structure function is modified in a nuclear medium. This modification, known as the *EMC effect*, is reflected in the ratio of the unpolarized structure function of a bound hadron to that in free space showing

* E-mail: phutauruk@gmail.com

† E-mail: terry.mart@sci.ui.ac.id

‡ E-mail: kazuo.tsushima@gmail.com, kazuo.tsushima@cruzeirodosul.edu.br

less than unity [28], in particular at the large Bjorken- x region. Since then, studies of hadron structure and properties in the nuclear medium have expanded significantly (see Refs. [27, 29, 30] and references therein). This has primarily motivated us to study the ρ^+ meson EMFFs in the nuclear medium, which constitutes the central focus of the present work.

The ρ mesons have interesting internal quark dynamic features compared to those of the pions. For instance, even though both π^+ and ρ^+ mesons consist of the u and \bar{d} light dressed quarks and antiquarks, their physical masses, and internal structures are much different because of the spin interactions of the dressed quark and antiquark contents inside the mesons. This difference exhibits that the ρ meson with mass $m_\rho = 0.770$ GeV has spin-1 and odd parity $J^P = 1^-$, and the pion with mass $m_\pi = 0.140$ GeV has spin-0 and odd parity $J^P = 0^-$. Delving deeper into the ρ meson internal structure will lead us to a better understanding of the contribution of quarks or quark dynamics to its internal structure, and one can gain new insight into physics features based on QCD. So far, to gain a better understanding of the role of the nuclear medium on hadron structure and QCD properties in the medium, several studies have been performed using different theoretical models and approaches in Refs. [21, 31–37], in particular for the pion EMFFs. This is supported by the availability of experimental data for the free space pion EMFFs, even for only the intermediate Q^2 range, where ($Q^2 = -q^2 > 0$) is the negative of squared four-momentum transfer. However, experimental (empirical) data for the ρ meson EMFFs in free space or in the nuclear medium are still scarce compared to those for the pion. In the past, several experiments have been performed at the CERN SPS through the CERES/NA45 collaboration [38], CLAS g7 at JLAB [39, 40], and KEK Proton-Synchrotron [41, 42] to measure or extract the ρ meson properties in the nuclear medium, such as the mass, the spectral density function, and the decay width. Besides the experimental efforts, extensive theoretical studies have been carried out to investigate the properties of ρ mesons using various models and approaches, such as QCD sum rule (QCDSR) [43, 44], inverse QCD sum rule (IQCDSR) [45], chiral perturbation theory (ChPT) [46], generalized Nambu–Jona-Lasinio (GNJL) model [47], vector meson dominance (VMD) model [48–50], and dispersion relation [51]. These studies have been performed mostly on the in-medium ρ meson properties focusing on the chiral symmetry restoration, while a study of the ρ meson EMFFs in the nuclear medium is still scarce in the literature.

Recently, investigations of the free-space ρ -meson properties, such as its electromagnetic form factors (EMFFs), including the charge radius, magnetic moment, and quadrupole moment, have been extended in order to study their behavior in the nuclear medium [52]. The authors of Ref. [52] reported interesting features of the ρ meson EMFFs in the nuclear medium, which were calculated in a hybrid model; combining the light front constituent quark model (LFCQM) and quark-meson coupling (QMC) model. They found that the quadrupole form factor, $G_Q(Q^2)$, exhibits intriguing behavior in the nuclear medium. In particular, at low momentum transfer ($Q^2 \simeq 3 \text{ GeV}^2$), the values of $G_Q(Q^2)$ at $\rho_B/\rho_0 = 0.25$ and 0.50 intersect with the free-space result at $\rho_B/\rho_0 = 0.0$. This notable feature has motivated us to further investigate the ρ^+ meson EMFFs in the nuclear medium to better understand the underlying origin and implications of the behavior in the quadrupole form factor.

In the present study, using a consistent treatment approach, we systematically investigate the ρ^+ meson EMFFs incorporating the charge/electric $G_C(Q^2)$, the magnetic moment $G_M^*(Q^2)$, and the quadrupole moment $G_Q^*(Q^2)$ in symmetric nuclear matter within the framework of the covariant NJL model using the Schwinger proper time regularization scheme—simulating the quark confinement, where the medium effect is also calculated within the NJL model at the quark level [53]. The NJL model has been successfully employed in describing the hadron internal structures in free space and nuclear medium, e.g., the ρ meson EMFFs [13, 54], PDF [33], and ρ meson TMD-PDFs [23]. In this work, we compute the ρ^+ meson effective mass, in-medium ρ meson-quark coupling constant, and in-medium modifications of the ρ^+ meson EMFFs: charge radius, magnetic moment, and quadrupole moment in the NJL model. As a result, we find that the ρ meson effective mass decreases as the nuclear matter density increases. The reduction in the ρ meson mass at $\rho_B/\rho_0 = 1.0$ with $\rho_0 = 0.16 \text{ fm}^{-3}$ relative to that in free space is about 10%, which is consistent with that obtained by the QCDSR in Ref. [43], and very recent analysis using the IQCDSR in Ref. [45], which are approximated by (10-20)%. However, our result in the ρ mass reduction is rather different from that obtained in the hybrid model of Ref. [52], where they reported the reduction of about 33%. For the ρ meson-quark coupling constant, we find that it decreases as the nuclear matter density increases. In this study, we also find that the in-medium charge radius and quadrupole moment form factors of the ρ^+ meson increase as the nuclear matter density increases, while the in-medium magnetic moment form factor decreases.

This paper is organized as follows. In Sec. II, we briefly describe the free space ρ meson properties and structure in the covariant NJL model with the help of the Schwinger proper-time regularization scheme to simulate the quark confinement, mimicking QCD properties. Section III describes the symmetric nuclear matter in the NJL model and the calculations of the light quark effective masses. We then present the mathematical expression of the ρ meson properties in the nuclear medium in Sec. IV, while a formulation of the ρ meson EMFFs in the nuclear medium is presented in Sec. V. Section VI presents the numerical results for the ρ meson properties in the nuclear medium and free space. A summary and conclusion are devoted to Sec. VII.

II. FREE SPACE ρ MESON PROPERTIES

In this section, we present the description of the SU(2) flavor NJL model effective Lagrangian, in addition to the free space quark and ρ meson properties in the NJL model.

A. SU(2) NJL Lagrangian

The NJL model is a Poincaré-covariant quantum field theory-based model that shares QCD's main properties at low energy scales. For instance, the NJL model encapsulates the emergent features of QCD, such as the dynamical chiral symmetry breaking and confinement in some versions, like the presently used one. The dynamical chiral symmetry is clearly shown in the NJL model through the chiral condensate in the NJL gap equation, as the order parameter of the chiral symmetry breaking, which dynamically generates dressed quark mass from the bare (current) quark mass. As the original NJL model is not a confining model, the confinement in the present study is described through the Schwinger proper-time regularization scheme, which completely removes the unphysical threshold that allows the hadron decay into quarks. An SU(2) flavor symmetric NJL model effective Lagrangian can be written in terms of the four-fermion contact interactions, where the gluons are integrated out and absorbed into the coupling constants with dimension, given by [55]

$$\mathcal{L}_{\text{NJL}} = \bar{\psi}_q (i\partial - \hat{m}_q) \psi_q + \frac{1}{2} G_\pi \left[(\bar{\psi}_q \psi_q)^2 - (\bar{\psi}_q \vec{\tau} \gamma_5 \psi_q)^2 \right] - \frac{1}{2} G_\omega (\bar{\psi}_q \gamma^\mu \psi_q)^2 - \frac{1}{2} G_\rho \left[(\bar{\psi}_q \gamma^\mu \vec{\tau} \psi_q)^2 + (\bar{\psi}_q \gamma^\mu \gamma_5 \vec{\tau} \psi_q)^2 \right], \quad (1)$$

where the $\psi_q^T = (\psi_u, \psi_d)$ represents the quark field with flavor $q = (u, d)$, $\vec{\tau}$ is the Pauli matrices, and $\hat{m}_q = \text{diag}(m_u, m_d)$ is the current quark mass matrix. It is worth noting that one group of the four-fermion interaction terms is proportional to the coupling constant G_π , which governs the strength of the direct terms of the antiquark-quark interaction in the scalar and pseudoscalar channels, and is responsible for the dynamical chiral symmetry breaking (DCSB). The constants G_ω and G_ρ turn out to represent the ω and ρ meson coupling constants, respectively.

Using the mean-field approximation, we evaluate the dressed quark masses through the quark self-energy interaction. The gap equation in the Schwinger proper-time regularization scheme can be written as

$$\begin{aligned} M_q &= m_q + 12iG_\pi \int \frac{d^4 k}{(2\pi)^4} \text{Tr}[S_q(k)], \\ &= m_q - 4G_\pi \langle \bar{\psi}_q \psi_q \rangle = m_q + \frac{3G_\pi M_q}{\pi^2} \int_{\tau_{\text{UV}}}^{\tau_{\text{IR}}} \frac{d\tau}{\tau^2} e^{-\tau M_q^2}, \end{aligned} \quad (2)$$

where $\tau_{\text{UV}} = \Lambda_{\text{UV}}^{-2}$ and $\tau_{\text{IR}} = \Lambda_{\text{IR}}^{-2}$ denote the ultraviolet (UV) and infrared (IR) integration limits, respectively. The IR value is fixed at $\Lambda_{\text{IR}} = 0.24$ GeV, corresponding to Λ_{QCD} , while the UV value Λ_{UV} is determined by fitting the pion mass ($m_\pi = 0.14$ GeV) and decay constant ($f_\pi = 0.093$ GeV). In other words, Λ_{UV} and Λ_{IR} are known as the regularization scales (regulators) of the NJL model. M_q is the (dynamical) dressed quark mass for quark flavor q , and the trace, "Tr", appearing in the above, operates only over the Dirac indices. The quark condensate is denoted by $\langle \bar{\psi}_q \psi_q \rangle$, which is known as an order parameter of chiral symmetry breaking. The dressed quark propagator for different flavors of q is defined by

$$S_q^{-1}(k) = \not{k} - M_q + i\epsilon, \quad (3)$$

where, $\epsilon > 0$, and infinitesimal as usual. The formation of the (dressed quark)-(dressed antiquark) bound ρ meson state can be obtained by solving the Bethe-Salpeter equation (BSE) in the random phase approximation, which is equivalent to the ladder approximation. The solution to BSE in the vector channel is given by a two-body t -matrix of the interaction channel. The summation of the bubble diagram for the pion and ρ meson from infinite interaction can be written as

$$t_\pi(p^2) = \frac{-2iG_\pi}{1 + 2G_\pi \Pi_\pi(p^2)}, \quad t_{\rho(\omega)}^{\mu\nu}(p^2) = \gamma^\mu \left(\frac{-2iG_{\rho(\omega)}}{1 + 2G_{\rho(\omega)} \Pi_{\rho(\omega)}(p^2)} \right) \gamma^\nu \left[g^{\mu\nu} + 2G_{\rho(\omega)} \Pi_{\rho(\omega)}(p^2) \frac{p^\mu p^\nu}{p^2} \right]. \quad (4)$$

The polarization insertions (bubble diagrams) for the pion and vector mesons are given by

$$\begin{aligned} \Pi_\pi(p^2) \delta_{ab} &= 3i \int \frac{d^4 k}{(2\pi)^4} \text{Tr} \left[\gamma_5 \tau_a S_q(p+k) \gamma_5 \tau_b S_q(k) \right], \\ \Pi_{\rho(\omega)}(p^2) P^{\mu\nu} \delta_{ab} &= 3i \int \frac{d^4 k}{(2\pi)^4} \text{Tr} \left[\gamma^\mu \tau_a S_q(p+k) \gamma^\nu \tau_b S_q(k) \right], \end{aligned} \quad (5)$$

respectively, where $P^{\mu\nu} = \left(g^{\mu\nu} - \frac{p^\mu p^\nu}{p^2}\right)$, and the trace operates over the Dirac and flavor indices. Note that the ρ meson mass is defined by the pole position in the corresponding two-body t -matrix.

B. ρ meson masses

The pion, ρ , and ω meson masses can be straightforwardly determined from the pole positions of the corresponding t -matrix in Eq. (4), and one has

$$1 + 2G_\pi \Pi_\pi(p^2 = m_\pi^2) = 0, \quad (6)$$

$$1 + 2G_\rho \Pi_\rho(p^2 = m_\rho^2) = 0, \quad (7)$$

$$1 + 2G_\omega \Pi_\omega(p^2 = m_\omega^2) = 0, \quad (8)$$

where they are determined by the bound state pole positions of the t -matrix. The m_π , m_ρ , and m_ω in Eqs. (6)-(8) denote the masses of the pion, rho, and omega mesons, respectively.

To determine the meson-quark coupling constant, we expand the t -matrix in Eq. (4) around the pole $p^2 = m_{\rho(\omega)}^2$, and we can obtain the meson wave function renormalization constants or the meson-quark coupling constants by using

$$Z_\pi^{-1} = \left[g_{\pi qq}\right]^{-2} = -\frac{\partial \Pi_\pi(p^2)}{\partial p^2} \bigg|_{p^2=m_\pi^2}, \quad (9)$$

$$Z_{\rho(\omega)}^{-1} = \left[g_{\rho(\omega) qq}\right]^{-2} = -\frac{\partial \Pi_{\rho(\omega)}(p^2)}{\partial p^2} \bigg|_{p^2=m_{\rho(\omega)}^2}, \quad (10)$$

where $g_{\pi qq}$ and $g_{\rho(\omega) qq}$ represent the corresponding meson-quark coupling constants. Next, we extend these free-space NJL expressions to the nuclear medium in Sec. IV. Before explaining the properties of the ρ meson in the nuclear medium, in Sec. III, we explain the nuclear matter description in the NJL model.

III. NJL MODEL NUCLEAR MATTER

In this section, we present the extension of the SU(2) flavor NJL model Lagrangian to symmetric nuclear matter, applying the Fierz transformation [56], where the four-fermion interactions can be decomposed as a chiral symmetric linear combination of the form $\sum_i G_i (\bar{\psi}_q \Gamma_i \psi_q)^2$. Note that the NJL nuclear matter model is characterized by the nuclear (baryon) density ρ_B . After performing the quark bilinear¹ into the effective NJL Lagrangian in Eq. (1), one has [31, 53]

$$\mathcal{L}_{\text{NM-NJL}} = \bar{\psi}_q (i\partial - M_q - \not{V}) \psi_q - \frac{(M_q - m_q)^2}{4G_\pi} + \frac{V_\mu V^\mu}{2G_\omega} + \mathcal{L}_I, \quad (11)$$

where \mathcal{L}_I stands for the interaction Lagrangian. Through the Fierz transformation and charge conjugation, \mathcal{L}_I in Eq. (11) is decomposed into a sum of the qq interactions of the isoscalar-scalar ($0^+, T=0$) and isovector-axial vector ($1^+, T=1$), so that \mathcal{L}_I can be written as

$$\mathcal{L}_{I,qq} = G_s [\bar{\psi}_q \gamma_5 C \tau_2 \beta_A \bar{\psi}_q^T] [\psi^T C^{-1} \gamma_5 \tau_2 \beta_A \psi_q] + G_a [\bar{\psi}_q \gamma_\mu C \tau_i \tau_2 \beta_A \bar{\psi}_q^T] [\psi_q^T C^{-1} \gamma^\mu \tau_2 \tau_i \beta_A \psi_q], \quad (12)$$

where $\beta_A = \sqrt{\frac{3}{2}} \lambda_A$ with $A = 2, 5, 7$, $C = i\gamma_2 \gamma_0$, and G_s and G_a are the coupling constants of the scalar and axial vector qq interactions, respectively. It is worth noting that the scalar coupling constant G_s is tuned to reproduce the free nucleon mass. The isoscalar-vector mean field and the dynamical effective quark mass can be, respectively, introduced by

$$V^\mu = 2G_\omega \langle \rho_B | \bar{\psi}_q \gamma^\mu \psi_q | \rho_B \rangle = 2\delta^{0\mu} G_\omega \langle \psi_q^\dagger \psi_q \rangle, \quad (13)$$

$$M_q = m_q - 2G_\pi \langle \rho_B | \bar{\psi}_q \psi_q | \rho_B \rangle, \quad (14)$$

¹ The quark bilinear $(\bar{\psi}_q \psi_q)$ and $(\bar{\psi}_q \gamma^\mu \psi_q)$ can be decomposed as $\langle \rho_B | \bar{\psi}_q \psi_q | \rho_B \rangle + (\bar{\psi}_q \psi_q)$ and $\langle \rho_B | \bar{\psi}_q \gamma^\mu \psi_q | \rho_B \rangle + (\bar{\psi}_q \gamma^\mu \psi_q)$. For details, see Ref. [53].

TABLE I. Density dependence of constituent quark mass, ρ meson mass, ρ decay constant, ρ -quark coupling constant, ρ^+ magnetic moment, ρ^+ quadrupole moment, ρ^+ charge radius, quark condensate, and nucleon effective mass calculated in the NJL model. All units are in MeV. The units of Q_ρ^* and $\langle r_\rho^* \rangle$ are in fm² and fm, respectively.

ρ_B/ρ_0	M_q^*	m_ρ^*	$g_{\rho qq}^*$	$\mu_\rho^*(\mu_N)$	Q_ρ^*	$\langle r_\rho^* \rangle$	$-\langle \bar{u}u \rangle^{*1/3}$	M_N^*
0.00	400	770	2.638	2.53	-0.057	0.67	171	934.36
0.50	360	726	2.537	2.41	-0.065	0.71	165	842.54
1.00	328	694	2.459	2.33	-0.071	0.75	160	778.03
1.50	306	673	2.410	2.28	-0.076	0.77	156	738.98
2.00	289	658	2.373	2.26	-0.080	0.79	153	715.34

where the vector potential can be defined as $V = (V_0, \mathbf{0})$ in symmetric nuclear matter at rest. Then, by the stable (minimum) condition $\partial \mathcal{E}/\partial V_0 = 0$, the value of V_0 is given as $V_0 = 6G_\omega \rho_B$, where the $\rho_B = 2p_F^3/3\pi^2$ stands for the baryon number density (nuclear matter density). Notably, the dynamical quark mass for fixed baryon density must satisfy the stable (minimum) condition $\partial \mathcal{E}/\partial M_q = \frac{(M_q - m_q)}{2G_\pi} + \langle \rho_B | \bar{\psi}_q \psi_q | \rho_B \rangle = 0$ to have a similar in-medium dynamical quark mass as in Eq. (13).

Using the standard hadronization technique [53], the effective potential for symmetric nuclear matter can be determined from the effective NJL Lagrangian. In the mean-field approach (MFA), the energy density of the symmetric nuclear matter is introduced by

$$\mathcal{E} = \mathcal{E}_V - \frac{V_0^2}{4G_\omega} + 4 \int \frac{d^3 p}{(2\pi)^3} \Theta(p_F - |\mathbf{p}|) \epsilon_N, \quad (15)$$

where $\epsilon_N = \sqrt{M_N^{*2} + \mathbf{p}^2} + 3V_0 \equiv E_N + 3V_0$ with $M_N^*(M_q \equiv M_q^*)$ is the in-medium nucleon mass obtained from the pole of the quark-diquark t -matrix and the nucleon Fermi momentum p_F , which is given by $p_F^2 = [(\mu_N - 3V_0)^2 - M_N^{*2}]$, with μ_N being the chemical potential of nucleon. The vacuum contribution of the quark is given by

$$\mathcal{E}_V = 12i \int \frac{d^4 k}{(2\pi)^4} \ln \left(\frac{k^2 - M_q^2 + i\epsilon}{k^2 - M_0^2 + i\epsilon} \right) + \frac{(M_q - m_q)^2}{4G_\pi} - \frac{(M_0 - m_q)^2}{4G_\pi}, \quad (16)$$

where M_0 is the vacuum constituent quark mass at zero density. Using the expression of the energy density for the NJL symmetric nuclear matter, the (negative of) energy per nucleon for symmetric nuclear matter with free space nucleon mass M_{N0} can be given by

$$\frac{E_B}{A} = \frac{\mathcal{E}}{\rho_B} - M_{N0}. \quad (17)$$

As mentioned before, the stability of symmetric nuclear matter of the NJL model is guaranteed by reproducing the energy per nucleon $E_B/A = -15.7$ MeV at saturation density $\rho_0 = 0.16$ fm⁻³. Now we study the ρ meson properties in the nuclear medium by using the quark properties in symmetric nuclear matter calculated by the NJL model as inputs.

IV. ρ MESON IN NUCLEAR MEDIUM

Here, we present the formulation of the in-medium properties of the ρ meson. The NJL dynamical quark mass in symmetric nuclear matter is expressed as

$$M_q^* = m_q + 4iG_\pi \text{Tr}[S_q^*(p^*)], \quad (18)$$

where M_q^* represents the dynamical quark effective masses, which corresponds to M_q in Eq. (14). The coupling constant G_π represents the scalar interaction strength and is taken to be the same as in free space. Note that here the Λ_{IR} is set to zero in the deconfined phase, when we consider a nuclear (quark) matter. This implies that nucleon

decay into quarks may occur at an unphysical threshold. The in-medium dressed light quark propagators in Eq. (18) can be expressed by

$$S_q^*(k^*) = \frac{(\not{k}^* + M_q^*)}{(k^{*2} - M_q^{*2} + i\epsilon)}, \quad (19)$$

where the asterisk symbol in Eq. (19) stands for the in-medium quantity which enters the light quark momentum k^μ by $k^{*\mu} = k^\mu + V^\mu$, due to the vector meson mean field $V^\mu = (V^0 = V_0, \mathbf{0})$. Note that the medium modifications of the space component of the light quark momentum $k^{*\mu}$ can be ignored, since the contribution is insignificant [57]. It is to be noted that, after substituting the in-medium modifications of the quark propagator into the constituent quark mass formula in Eq. (18), we can shift the variable of the integral to eliminate the vector potential that enters the light quark momentum.

We now present the description of the bound state of the mesons in the nuclear medium. Shortly, the in-medium reduced t -matrices for the π and $\rho(\omega)$ mesons are respectively obtained by

$$t_\pi^*(p^*) = \frac{-2iG_\pi}{1 + 2G_\pi \Pi_\pi^*(p^{*2})}, \quad t_{\rho(\omega)}^{*\mu\nu}(p^*) = \frac{-2iG_\rho}{1 + 2G_\rho \Pi_V^*(p^{*2})} \left[g^{\mu\nu} + 2G_{\rho(\omega)} \Pi_{\rho(\omega)}^*(p^{*2}) \frac{p^{*\mu} p^{*\nu}}{p^2} \right], \quad (20)$$

where G_ρ is the four-fermion coupling constant for the vector meson channels and the polarization insertions, which are the so-called bubble diagrams in the nuclear medium, can be introduced by

$$\begin{aligned} \Pi_\pi^*(p^{*2}) &= 6i \int \frac{d^4k}{(2\pi)^4} \text{Tr} \left[\gamma_5 S_q^*(k^*) \gamma_5 S_q^*(k^* + p^*) \right], \\ \Pi_{\rho(\omega)}^*(p^{*2}) P_T^{\mu\nu} &= 6i \int \frac{d^4k}{(2\pi)^4} \text{Tr} \left[\gamma^\mu S_q^*(k^*) \gamma^\nu S_q^*(k^* + p^*) \right], \end{aligned} \quad (21)$$

where $P_T^{\mu\nu} = (g^{\mu\nu} - q^\mu q^\nu / q^2)$, and Tr only operates to the Dirac matrices. After extracting the polarization insertion for the vector mesons, we can straightforwardly determine the in-medium meson masses for the π and $\rho(\omega)$ mesons as the pole positions of the t -matrix, which are given by

$$1 + 2G_\pi \Pi_\pi^*(p^{*2} = m_\pi^{*2}) = 0, \quad (22)$$

$$1 + 2G_{\rho(\omega)} \Pi_{\rho(\omega)}^*(p^{*2} = m_{\rho(\omega)}^{*2}) = 0, \quad (23)$$

where m_π^* , and $m_{\rho(\omega)}^*$ are the pion and vector meson $\rho(\omega)$ effective masses, respectively. Next, the pion-quark and $\rho(\omega)$ -quark coupling constants in the nuclear medium can be computed by taking the first derivative of the polarization insertion with respect to p^{*2} , which yields

$$[Z_\pi^*]^{-1} = [g_{\pi qq}^*]^{-2} = - \left. \frac{\partial \Pi_\pi^*(p^{*2})}{\partial p^{*2}} \right|_{p^{*2} = m_\pi^{*2}}, \quad (24)$$

$$[Z_{\rho(\omega)}^*]^{-1} = [g_{\rho(\omega) qq}^*]^{-2} = - \left. \frac{\partial \Pi_{\rho(\omega)}^*(p^{*2})}{\partial p^{*2}} \right|_{p^{*2} = m_{\rho(\omega)}^{*2}}. \quad (25)$$

In the next section, we discuss the formulation of the ρ meson EMFFs in the nuclear medium. Furthermore, we explain the in-medium modifications of the charge radius, the magnetic moment, and the quadrupole moment of the ρ meson, which represent the main goal of this work.

V. IN-MEDIUM ρ MESON EMFFS

Here we describe the ρ meson EMFFs in the nuclear medium in the covariant NJL model. Shortly, the generic expression for the electromagnetic current for the ρ meson can be parameterized in terms of three form factors,

$$\mathcal{J}_\rho^{\mu, \alpha\beta}(p'^*, p^*) = \left[g^{\alpha\beta} F_1^{*\rho}(Q^2) - \frac{q^{\alpha*} q^{\beta*}}{2m_\rho^{*2}} F_2^{*\rho}(Q^2) \right] (p'^* + p^*)^\mu - \left[q^{\alpha*} g^{\mu\beta} - q^{\beta*} g^{\mu\alpha} \right] F_3^{*\rho}(Q^2), \quad (26)$$

where the superscript of the Lorentz indices α and β respectively correspond to the polarizations of the incoming and outgoing ρ meson, while μ corresponds to the photon polarization. $F_1^{*\rho}(Q^2)$, $F_2^{*\rho}(Q^2)$, and $F_3^{*\rho}(Q^2)$ are the in-medium ρ meson EMFFs that we want to extract using the NJL model.

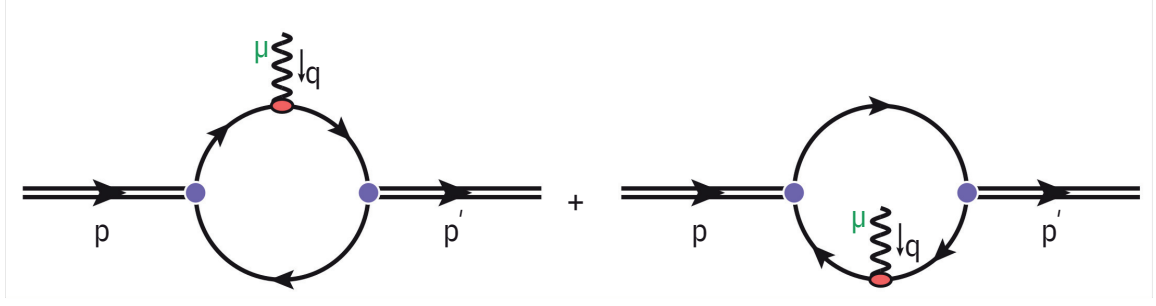


FIG. 1. Diagrammatic representations of the electromagnetic interaction with the ρ meson. In each panel, the BSE vertices are represented by the filled pair circles (purple), while the quark-photon vertex is represented by a filled oval (red), where we can assume that in the left figure, the photon hits the quark and, in the right figure, the photon hits the antiquark.

These form factors can be written in terms of three Sachs form factors for the ρ meson in the nuclear medium: the charge/electric form factor $[G_C^*(Q^2)]$, which is related to the charge distribution, magnetic form factor $[G_M^*(Q^2)]$, which is associated with the magnetization distribution, and quadrupole form factor $[G_Q^*(Q^2)]$, which reflects the shape or spatial symmetry of the ρ mesons. Explicitly, they are defined by

$$G_C^*(Q^2) = F_1^{*\rho}(Q^2) + \frac{2}{3}\eta G_Q^*(Q^2), \quad (27)$$

$$G_Q^*(Q^2) = F_1^{*\rho}(Q^2) + (1 + \eta)F_2^{*\rho}(Q^2) - F_3^{*\rho}(Q^2), \quad (28)$$

$$G_M^*(Q^2) = F_3^{*\rho}(Q^2), \quad (29)$$

where $\eta = Q^2/4m_\rho^{*2}$. It is worth noting that all form factors above are dimensionless.

In the NJL model, based on the diagrams in Fig. 1, the electromagnetic current for the ρ meson in the nuclear medium can be expressed by

$$\begin{aligned} \mathcal{J}_{\rho,ij}^{\mu,\alpha\beta}(p',p) &= i \int \frac{d^4k}{(2\pi)^4} \text{Tr} \left[\bar{\Gamma}_\rho^{\beta,j} S_q^*(p'^* + k^*) \Lambda_{\gamma Q}^{\mu*}(p',p) S_q^*(p^* + k^*) \Gamma_\rho^{\alpha,i} S_q^*(k^*) \right] \\ &+ i \int \frac{d^4k}{(2\pi)^4} \text{Tr} \left[\Gamma_\rho^{\alpha,i} S_q^*(k^* - p^*) \Lambda_{\gamma Q}^{\mu*}(p',p) S_q^*(k^* - p^*) \bar{\Gamma}_\rho^{\beta,j} S_q^*(k^*) \right], \\ &= 2i \int \frac{d^4k}{(2\pi)^4} \text{Tr} \left[\bar{\Gamma}_\rho^{\beta,j} S_q^*(p'^* + k^*) \Lambda_{\gamma Q}^{\mu*}(p',p) S_q^*(p^* + k^*) \Gamma_\rho^{\alpha,i} S_q^{*T}(-k^*) \right], \end{aligned} \quad (30)$$

where the trace, Tr , operates over the Dirac, color, and isospin indices, the superscript T stands for the transpose in the Dirac space, and $\Lambda_{\gamma Q}^{\mu*}(p',p)$ stands for the in-medium dressed quark-photon vertex, and is defined as

$$\Lambda_i^{(\text{BSE})\mu*}(Q^2) = \gamma^\mu F_{1i}^*(Q^2) + \frac{i\sigma^{\mu\nu}q_\nu}{2M} F_{2i}^*(Q^2), \quad (31)$$

where the subscript $i = (\rho, \omega)$ is the dressed quark form factor obtained from the inhomogeneous BSE. Note that $F_{1\omega}^*(Q^2) = F_{1\omega}^*(Q^2) = 1$ and $F_{2\rho}^*(Q^2) = F_{2\omega}^*(Q^2) = 0$, for the pointlike quark. This implies $F_{2Q}^*(Q^2) = \frac{1}{6}F_{2\omega}^*(Q^2) \pm \frac{1}{2}F_{2\rho}^*(Q^2) = 0$ where $Q = (U, D)$ (dressed quarks). However, $f_1^{*T}(Q^2)$, $f_2^{*T}(Q^2)$, and $f_3^{*T}(Q^2)$ are not zero as can be seen in Refs. [13, 54]. It is worth noting that $f_3^T(Q^2) = 0$ as it preserves charge conservation.

After full derivations and some calculations of the in-medium EM current for the ρ meson in the NJL model, Eq. (30), and comparing it with the current in Eq. (26), we can extract the ρ meson EMFFs in the nuclear medium. The final expressions for the ρ meson EMFFs in the NJL model are respectively given by

$$F_1^{*\rho}(Q^2) = [F_{1U}^*(Q^2) - F_{1D}^*(Q^2)] f_1^{V*}(Q^2) + [F_{2U}^*(Q^2) - F_{2D}^*(Q^2)] f_1^{*T}(Q^2), \quad (32)$$

$$F_2^{*\rho}(Q^2) = [F_{1U}^*(Q^2) - F_{1D}^*(Q^2)] f_2^{V*}(Q^2) + [F_{2U}^*(Q^2) - F_{2D}^*(Q^2)] f_2^{*T}(Q^2), \quad (33)$$

$$F_3^{*\rho}(Q^2) = [F_{1U}^*(Q^2) - F_{1D}^*(Q^2)] f_3^{V*}(Q^2) + [F_{2U}^*(Q^2) - F_{2D}^*(Q^2)] f_3^{*T}(Q^2), \quad (34)$$

where the subscripts 1, 2, and 3 stand for the three form factors given in Eq. (26) and f_i^{V*} is the body form factor for vector part with $i = 1, 2, 3$. The vector body form factors in the Schwinger proper time regularization scheme are

given by

$$f_1^{V*}(Q^2) = -\frac{3g_{\rho qq}^{*2}}{16\pi^2} \int_{\tau_{UV}}^{\tau_{IR}} d\tau \int_0^1 dx \int_{-x}^x dy \left(\frac{4}{\tau} (1-x) - 2xm_\rho^{*2} \right) \exp \left[-\tau((x^2-x)m_\rho^{*2} + \frac{1}{4}(x^2-y^2)Q^2 + M_q^{*2}) \right] \\ + \frac{3g_{\rho qq}^{*2}}{4\pi^2} \int_{\tau_{UV}}^{\tau_{IR}} d\tau \int_0^1 dx \frac{\exp \left[-\tau((x-x^2)Q^2 + M_q^{*2}) \right]}{\tau}, \quad (35)$$

$$f_2^{V*}(Q^2) = \frac{3g_{\rho qq}^{*2}m_\rho^{*2}}{4\pi^2} \int_{\tau_{UV}}^{\tau_{IR}} d\tau \int_0^1 dx \int_{-x}^x dy (x^2-y^2)(1-x) \exp \left[-\tau((x^2-x)m_\rho^{*2} + \frac{1}{4}(x^2-y^2)Q^2 + M_q^{*2}) \right], \quad (36)$$

$$f_3^{V*}(Q^2) = -\frac{3g_{\rho qq}^{*2}}{16\pi^2} \int_{\tau_{UV}}^{\tau_{IR}} d\tau \int_0^1 dx \int_{-x}^x dy \left[\frac{4}{\tau} (x+1) - 2x(1+2x)m_\rho^{*2} - (x^2-y^2)Q^2 \right] \\ \times \exp \left[-\tau((x^2-x)m_\rho^{*2} + \frac{1}{4}(x^2-y^2)Q^2 + M_q^{*2}) \right] \\ + \frac{9g_{\rho qq}^{*2}}{4\pi^2} \int_0^1 dx \int_{\tau_{UV}}^{\tau_{IR}} \frac{d\tau}{\tau} \exp \left[-\tau((x-x^2)Q^2 + M_q^{*2}) \right], \quad (37)$$

while the tensor body form factors are given by

$$f_1^{T*}(Q^2) = -\frac{3g_{\rho qq}^{*2}Q^2}{16\pi^2} \int_0^1 dx \int_{-x}^x dy \int_{\tau_{UV}}^{\tau_{IR}} d\tau \exp \left[-\tau((x^2-x)m_\rho^{*2} + \frac{1}{4}(x^2-y^2)Q^2 + M_q^{*2}) \right], \quad (38)$$

$$f_2^{T*}(Q^2) = \frac{3g_{\rho qq}^{*2}m_\rho^{*2}}{4\pi^2} \int_0^1 dx \int_{-x}^x dy \int_{\tau_{UV}}^{\tau_{IR}} d\tau (1-x) \exp \left[-\tau((x^2-x)m_\rho^{*2} + \frac{1}{4}(x^2-y^2)Q^2 + M_q^{*2}) \right], \quad (39)$$

$$f_3^{T*}(Q^2) = -\frac{3g_{\rho qq}^{*2}}{16\pi^2} \int_0^1 dx \int_{-x}^x dy \int_{\tau_{UV}}^{\tau_{IR}} d\tau \left[xQ^2 - 2m_\rho^{*2} \right] \exp \left[-\tau((x^2-x)m_\rho^{*2} + \frac{1}{4}(x^2-y^2)Q^2 + M_q^{*2}) \right] \\ + \frac{3g_{\rho qq}^{*2}}{4\pi^2} \int_0^1 dx \int_{\tau_{UV}}^{\tau_{IR}} \frac{d\tau}{\tau} \exp \left[-\tau((x-x^2)Q^2 + M_q^{*2}) \right]. \quad (40)$$

The inhomogeneous BSE-dressed quark form factors in the nuclear medium can be defined by

$$F_{1U}^*(Q^2) = \frac{1}{6}F_{1\omega}^*(Q^2) + \frac{1}{2}F_{1\rho}^*(Q^2), \quad (41)$$

$$F_{1D}^*(Q^2) = \frac{1}{6}F_{1\omega}^*(Q^2) - \frac{1}{2}F_{1\rho}^*(Q^2), \quad (42)$$

$$F_{2U}^*(Q^2) = \frac{1}{6}F_{2\omega}^*(Q^2) + \frac{1}{2}F_{2\rho}^*(Q^2), \quad (43)$$

$$F_{2D}^*(Q^2) = \frac{1}{6}F_{2\omega}^*(Q^2) - \frac{1}{2}F_{2\rho}^*(Q^2), \quad (44)$$

where the dressed quark form factors are given by $F_{1\rho(1\omega)}^*(Q^2) = 1/[1 + 2G_{\rho(\omega)}\Pi_{\rho(\omega)}^*(p^{*2})]$, $F_{2\rho(2\omega)}^*(Q^2) = 0$, and $F_{1\rho}^*(Q^2)$ and $F_{1\omega}^*(Q^2)$ have poles at $p^{*2} = m_\rho^{*2}$ and $p^{*2} = m_\omega^{*2}$, respectively. It is worth noting that the BSE kernel of the NJL model does not generate the Pauli form factors $F_{2\rho(2\omega)}^*(Q^2)$ because of the absence of the tensor-tensor four-fermion interaction in the present approach.

Through the ρ meson EMFFs in nuclear medium, we can straightforwardly compute the static electromagnetic quantities of the ρ meson in the nuclear medium, such as the magnetic moment μ_ρ^* , quadrupole moment Q_ρ^* , and the squared charge radius $\langle r_C^{*2} \rangle$. These static quantities can be determined, respectively, by

$$\mu_\rho^* = G_M^*(Q^2=0) \frac{M_N^*}{m_\rho^*}, \quad (45)$$

$$Q_\rho^* = \frac{G_Q^*(Q^2=0)}{m_\rho^{*2}}, \quad (46)$$

$$\langle r_C^{*2} \rangle = -6 \frac{\partial G_C^*(Q^2)}{\partial Q^2} \bigg|_{Q^2=0}, \quad (47)$$

where M_N^* stands for the effective nucleon mass. The values for both M_N^* and m_ρ^* masses for various matter densities are given in Table I. It is worth noting that the charge is normalized by $G_C^*(Q^2=0) = 1$.

VI. NUMERICAL RESULT

Here, we present the numerical results for the ρ meson properties and their EMFFs, such as the charge radius $\langle r_\rho^* \rangle \equiv \langle r_C^{*2} \rangle^{1/2}$ (See Eq. (47)), the charge form factor $G_C^*(Q^2)$, magnetic form factor $G_M^*(Q^2)$, and quadrupole moment form factor $G_Q^*(Q^2)$ in the nuclear medium. The NJL model parameter used in the present work is G_π , G_ω , G_ρ , G_a , and G_s , as used in Refs. [33, 34, 53]. In this work, the regularization parameter Λ_{IR} in the Schwinger proper-time regularization scheme is fixed at 240 MeV, which is comparable to Λ_{QCD} , while the free space (vacuum) constituent quark mass is taken as $M_0 = 400$ MeV for u and d quarks.

The remaining free space parameters are fitted to the physical pion mass $m_\pi = 140$ MeV, physical kaon mass $m_K = 495$ MeV, nucleon mass $M_N = M_{N0} = 940$ MeV, and ρ meson mass $m_\rho = 770$ MeV, together with the pion weak-decay constant $f_\pi = 93$ MeV. The fitted results give an ultraviolet cutoff $\Lambda_{\text{UV}} = 645$ MeV, pion coupling constant $G_\pi = 19.04 \times 10^{-6}$ MeV $^{-2}$, axial-vector diquark coupling constant $G_a = 2.8 \times 10^{-6}$ MeV $^{-2}$, scalar diquark coupling constant $G_s = 7.49 \times 10^{-6}$ MeV $^{-2}$, and strange constituent quark mass $M_s = 611$ MeV. The ϕ meson mass is taken $m_\phi = 1001$ MeV, scalar diquark mass $M_s = 687$ MeV, and axial diquark mass $M_a = 1027$ MeV. It is worth noting that the coupling constants G_s and G_a are determined by solving the Faddeev equation to reproduce the nucleon mass in vacuum, M_N , and axial coupling constant of nucleon $g_A = 1.267$, as employed in Ref. [53].

The parameters for symmetric nuclear matter are determined by fitting the (negative of) energy per nucleon, $E_B/A = -15.7$ MeV, at the saturation baryon density $\rho_0 = 0.16$ fm $^{-3}$. This yields a value of $G_\omega = 6.03 \times 10^{-6}$ MeV $^{-2}$. The current quark mass value (in vacuum) for the up quark (and down quark) is taken as $m_u = m_d = 16$ MeV (SU(2) isospin symmetry), while the current mass of the strange quark is set to $m_s = 356$ MeV, following Refs. [33, 34, 53].

A. In-medium ρ meson properties

Results for the ρ meson properties in nuclear medium are shown in Fig. 2(a)-(d). Evaluating the pole position of the t -matrix in Eq. (22), we obtain the ρ meson mass in nuclear medium, as depicted in Fig. 2(a). It shows that the ρ meson mass decreases as the nuclear matter density increases. A similar behavior was found in Refs. [52, 58], represented by the filled asterisk (red) data, where the in-medium ρ meson mass also decreases as the nuclear matter density increases. However, the magnitude is significantly different, in particular at $\rho_B/\rho_0 \gtrsim 0.5$. It is worth noting that in Ref. [52], they used ρ_0 is 0.15 fm $^{-3}$, which is different from the present work, $\rho_0 = 0.16$ fm $^{-3}$. The difference in the ρ meson mass in the nuclear medium is more pronounced at higher densities due to the strong attractive scalar potential in the QMC model, as clearly indicated in Fig. 2(a). We find that the ρ mass reduction relative to that in free space is approximately 10% at normal nuclear matter density $\rho_B/\rho_0 = 1.00$, which also may correspond to the amount of the chiral symmetry restoration. Our result is consistent with that obtained by the QCDSR of Ref. [43] and a very recent analysis in the IQCDSR of Ref. [45], which are about (10-20)% in the ρ mass reduction. However, our result in ρ mass reduction is rather different from that obtained in Ref. [52], which is approximated by 33%. The difference is probably related to a larger constituent light quark mass m_q used in the model of Ref. [52] (See Table I of the reference), where this value of $m_q = 430$ MeV was set to be able to have the "bound ρ meson state", yielding the larger g_σ and g_ω coupling constant values to reproduce the empirically extracted nuclear matter saturation properties in the QMC model.

In Fig. 2(b), we also show the dynamical quark effective mass in symmetric nuclear matter calculated in the NJL model that was described in Sec. III. It is worth noting that this in-medium dynamical quark mass was used as input to calculate the ρ meson mass in symmetric nuclear matter within the NJL model. As in the features of the in-medium ρ meson mass, the dynamical quark mass also decreases with increasing nuclear matter density. The trend of our results for the ρ meson and dynamical quark masses is consistent with other theoretical predictions [52], but different in magnitude, as clearly indicated in Fig. 2(b). We also compare our present result with that calculated in the QMC model reported in Ref. [52]. We find that the differences are more significant at higher densities. Again, these differences are expected due to a strong scalar attractive potential originated from the QMC model. We find that the reduction of the dynamical quark effective mass at $\rho_B/\rho_0 = 1.0$ relative to that in free space (vacuum) is approximately 18% (72 MeV). The reduction of the constituent quark mass at $\rho_B/\rho_0 = 0.9$ obtained in Ref. [52] is 40% (170 MeV), which is larger than our result. Note that to be exactly comparable with the present unit scale of $\rho_0 = 0.16$ fm $^{-3}$, the nuclear matter density has to be adjusted by a factor of 0.9375, for example, $\rho_B/\rho_0 = 0.9 \times (0.15/0.16) = 0.9 \times 0.9375 = 0.84375$, as shown in Figs. 2(a)-(b).

Next, we show the results of the ρ -quark coupling constant for different nuclear matter densities in Fig. 2(c). It is worth noting that the ρ -quark coupling constant is related to the ρ meson wave function renormalization constants, which are given in Eqs. (24) and (25). We find that the ρ -quark coupling constant decreases when the nuclear matter density increases. Furthermore, we found that the reduction of the ρ -quark coupling constant at normal nuclear

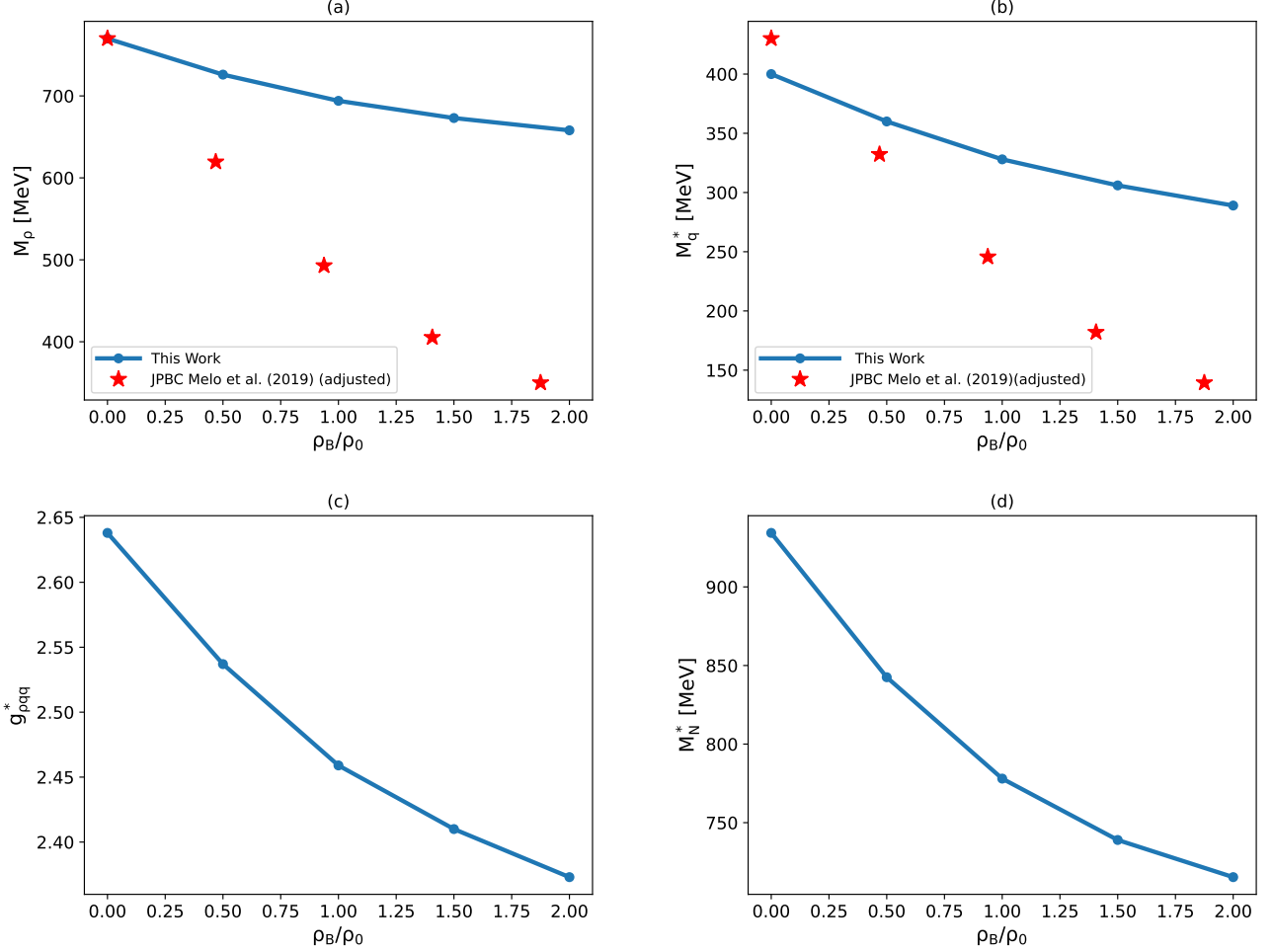


FIG. 2. Results for (a) ρ meson effective mass, (b) dynamical quark effective mass, (c) ρ -quark coupling constant, and (d) nucleon effective mass as a function of ρ_B/ρ_0 , where ρ_B and ρ_0 ($= 0.16 \text{ fm}^{-3}$) are respectively the baryon and saturation densities. Note that the in-medium ρ meson and dynamical effective quark masses represented by the filled asterisk (red) data are taken from Ref. [52]. Note that, as mentioned in the text, the results of Ref. [52] used $\rho_0 = 0.15 \text{ fm}^{-3}$ and thus, for an exact comparison with the present results ($\rho_0 = 0.16 \text{ fm}^{-3}$), we adjust the horizontal values of the filled asterisk (red) data multiplying by a factor of $(0.15/0.16) = 0.9375$. Additionally, the “hybrid” model of the ρ -meson in Ref. [52] can form the bound state ρ meson up to around $\rho_B/\rho_0 \simeq 0.9 \times 0.9375 = 0.84375$ in the present ρ_B/ρ_0 units. Thus, for larger nuclear matter densities, the in-medium ρ meson properties could not be calculated within the “hybrid model” in Ref. [52].

matter density relative to that in free space is about 7%.

Figure 2(d) shows the results of the nucleon effective mass as a function of the nuclear matter density. The nucleon effective mass is calculated in the NJL nuclear matter model described in Sec. III, which shows the unique features of the NJL model approach computed at the quark level. As a result, it shows that, as the nuclear matter density increases, the nucleon effective mass decreases, which is consistent with other theoretical predictions [52, 59]. The reduction of the nucleon effective mass at normal nuclear matter density relative to that in free space is about 17% (156 MeV). We note that the NJL model approach to nuclear matter reproduces the (negative of) energy for nuclear matter at saturation density $\rho_0 = 0.16 \text{ fm}^{-3}$, as explained in Ref. [53]. This indicates that the NJL model description of nuclear matter guarantees the nuclear matter stability, as empirically proven.

B. In-medium ρ meson EMFFs

Before presenting the results for the charge, magnetic moment, and quadrupole form factors of the ρ^+ meson in symmetric nuclear matter as well as in free space, we explore first the results of the BSE dressed up-quark form

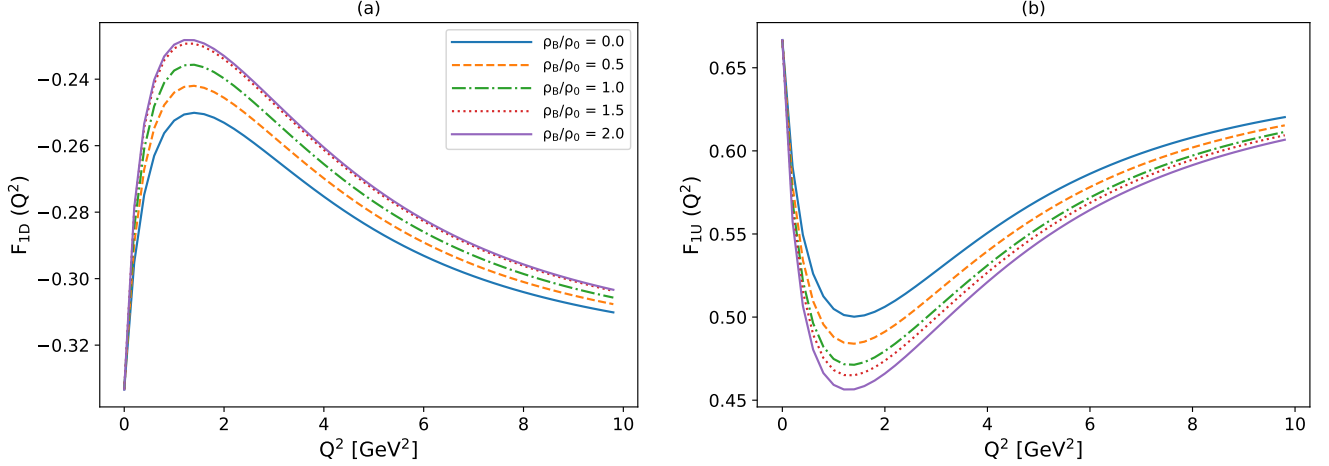


FIG. 3. Results for the BSE dressed quark form factors for different nuclear matter densities, (a) BSE dressed form factor of the down quark, $F_{1D}^*(Q^2)$, and (b) BSE dressed form factor of the up quark, $F_{1U}^*(Q^2)$ for different densities as a function of Q^2 .

factors² $F_{1U}^*(Q^2)$ and down-quark (antidown-quark can be obtained by multiplying by a factor of -1) form factors, $F_{1D}^*(Q^2)$, where the expression of this inhomogeneous BSE dressed quark form factors are formulated in Eq. (41).

Results for BSE dressed down-quark form factor $F_{1D}^*(Q^2)$ for different nuclear matter densities as a function of Q^2 are shown in Fig. 3(a), where we can see that $F_{1D}^*(Q^2)$ increases as the nuclear matter density increases. At $Q^2 = 0$ we have $F_{1D}^*(Q^2 = 0) = e_d = -1/3$, where e_d stands for the electric charge of the down quark. It is worth noting that this normalization value at $Q^2 = 0$ is normalized not only in free space but also in nuclear matter. Also, we find that $F_{1D}^*(Q^2)$ increases up to around $Q^2 \simeq 2 \text{ GeV}^2$ and begins to decrease as the Q^2 increases. It is worth noting that, in this work, we do not consider the pion loops contributions in the ρ meson EMFFs as in Refs. [13, 54], since we focus on the nuclear medium effects on the ρ meson EMFFs. The pion loop contribution to the ρ meson EMFFs in nuclear matter is expected to be insignificant, because the physical pion mass remains nearly unchanged in the nuclear medium, as indicated in Ref. [31] (and references therein).

As $Q^2 \rightarrow \infty$ in free space, the $F_{1D}^*(Q^2)$ does not go to zero, but it behaves as $F_{1D}^*(Q^2) \simeq e_d$. A similar feature is captured in the $F_{1D}^*(Q^2)$ in nuclear matter, where it also gives $F_{1D}^*(Q^2) \simeq e_d$ at $Q^2 \rightarrow \infty$. Such a behavior at larger Q^2 is consistent with the expectation results from asymptotic freedom of QCD [54]. We also compute the BSE dressed form factors for the up quark. The results for the $F_{1U}^*(Q^2)$ as a function of Q^2 for different nuclear matter densities are illustrated in Fig. 3(b). It is clearly shown that the behavior of $F_{1U}^*(Q^2)$ is rather different from that for $F_{1D}^*(Q^2)$, where the $F_{1U}^*(Q^2)$ decreases as the nuclear matter density increases. As a function of Q^2 , the $F_{1U}^*(Q^2)$ form factor decreases up to $Q^2 \simeq 2 \text{ GeV}^2$, and then increases at higher Q^2 , exhibiting an opposite trend to that of $F_{1D}^*(Q^2)$. It is worth noting that if the absolute value is taken, or the sign is changed for the dressed D quark form factor as $-F_{1D}^*(Q^2)$, the global behavior looks similar except for the magnitude difference with $F_{1U}^*(Q^2)$.

Figure 3(b) also shows that $F_{1U}^*(Q^2 = 0) = e_u = 2/3$, which is the value of the up quark electric charge. This value is reproduced in free space (vacuum) and nuclear matter, as clearly shown in Fig. 3(b) at $Q^2 = 0$. For larger Q^2 (goes to infinity), we find that $F_{1U}^*(Q^2 \rightarrow \infty) \simeq e_u$, which is consistent with what we expect as the QCD behavior in the asymptotic regime.

In computing the ρ meson EMFFs in a nuclear medium, the medium effects are also expected to influence the vector body form factors, as formulated in Eqs. (32)-(34). Results for the vector body form factors for different nuclear matter densities as a function of Q^2 are depicted in Fig. 4(a)-(c). It is worth noting that, in addition to the vector body form factors, in general, there also exist the tensor body form factors, which come from the tensor part of $\sigma^{\mu\nu} q_\nu / 2M$. However, in the present work, the contributions from the tensor body form factors vanish, because $F_{2Q}^*(Q^2)$ is zero, with the dressed quark $Q = (U, D)$.

Figure 4(a) shows that the $f_1^{*V}(Q^2)$ decreases as the nuclear matter density ρ_B/ρ_0 and Q^2 increase. Note that the

² In Ref. [13], $F_{1U}^*(Q^2)$ and $F_{1D}^*(Q^2)$ are usually written as $F_{1U}^{*\text{BSE}}(Q^2)$ and $F_{1D}^{*\text{BSE}}(Q^2)$, respectively, where the BSE superscript indicates that the form factors are uniquely determined in the BSE. In this work, we suppress it for simplicity.

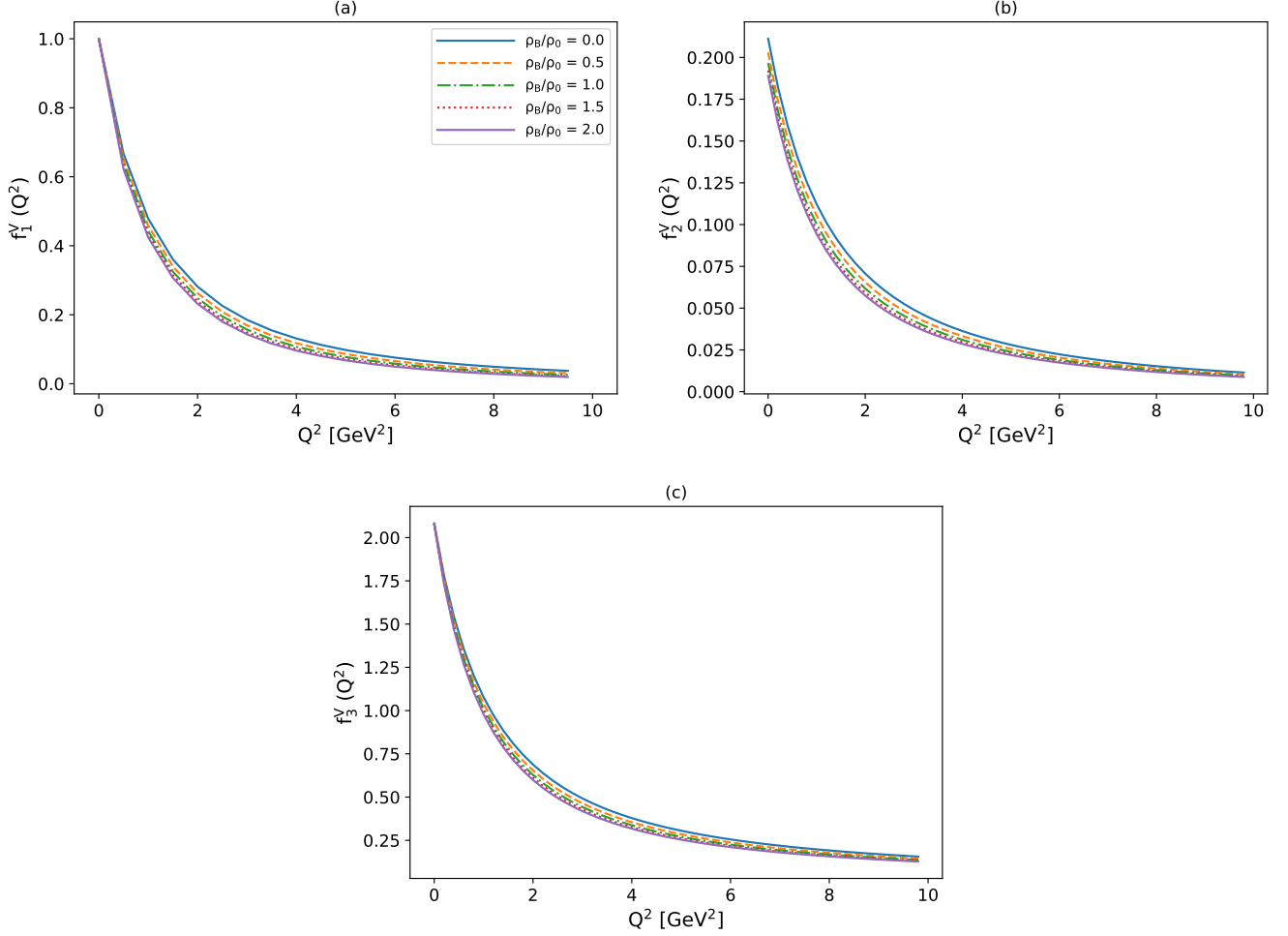


FIG. 4. Results of the vector body form factors, (a) $f_1^{*V}(Q^2)$, (b) $f_2^{*V}(Q^2)$, and (c) $f_3^{*V}(Q^2)$ for different nuclear matter densities as a function of Q^2 .

$f_1^V(Q^2)$ is unity at $Q^2 = 0$ in free space as well as in nuclear matter. This corresponds that $f_1^{*V}(Q^2)$ satisfies the charge conservation. Such a normalization condition is also found in Refs. [13, 54] for a free space case. Furthermore, Fig. 4(a) also exhibits that the change of $f_1^{*V}(Q^2)$ is more pronounced at higher densities.

In addition to the results for $f_1^{*V}(Q^2)$, we also show the results for the vector body form factors $f_2^{*V}(Q^2)$ for different nuclear matter densities as a function of Q^2 , as illustrated in Fig. 4(b). We find that the $f_2^{*V}(Q^2)$ also decreases as the ρ_B/ρ_0 and Q^2 increase. Also, the values of $f_2^{*V}(Q^2 = 0)$ decrease as the nuclear matter density increases. The reduction of $f_2^{*V}(Q^2 = 0)$ at $\rho_B/\rho_0 = 1.0$ is 6.87% in comparison to that for the free space. At higher density $\rho_B/\rho_0 = 2.0$, the decrease of $f_2^{*V}(Q^2 = 0)$ is 10.49%. In Fig. 4(c), we show our results for $f_3^{*V}(Q^2)$ as a function of Q^2 for different densities. In free space, $f_3^{*V}(Q^2 = 0) = 2.09$, which is the magnetic moment of the ρ^+ meson in the units of $e/(2m_\rho)$, where $e = 1$ and m_ρ are the natural units of the positron charge e and ρ meson mass, respectively. This value is rather larger than the canonical value [54]. In symmetric nuclear matter, the magnetic moment decreases as the nuclear matter density increases. For example, the values of $f_3^{*V}(Q^2 = 0) = 2.079$ at $\rho_B/\rho_0 = 1.0$. For $\rho_B/\rho_0 = 2.0$, we have $f_3^{*V}(Q^2 = 0) = 2.077$. Now we turn to discuss the results of the ρ^+ meson EMFFs, $F_1^\rho(Q^2)$, $F_2^\rho(Q^2)$, and $F_3^\rho(Q^2)$ in free space as well as in symmetric nuclear matter as depicted in Figs. 5(a)-(c). Results of $F_1^{*\rho}(Q^2)$ for different nuclear matter densities as a function of Q^2 are illustrated in Fig. 5(a). At $\rho_B/\rho_0 = 0.0$ (free space), our result on $F_1^\rho(Q^2)$ is consistent with that obtained in Ref. [54]. As the nuclear matter density and Q^2 increase, $F_1^{*\rho}(Q^2)$ decreases. It is worth noting that $F_1^{*\rho}(Q^2)$ always satisfies the normalization condition in free space and nuclear matter, i.e., $F_1^\rho(Q^2 = 0) = 1.0$.

In Fig. 5(b), we show the results of the $F_2^{*\rho}(Q^2)$ for different densities as a function of Q^2 . We find that the results

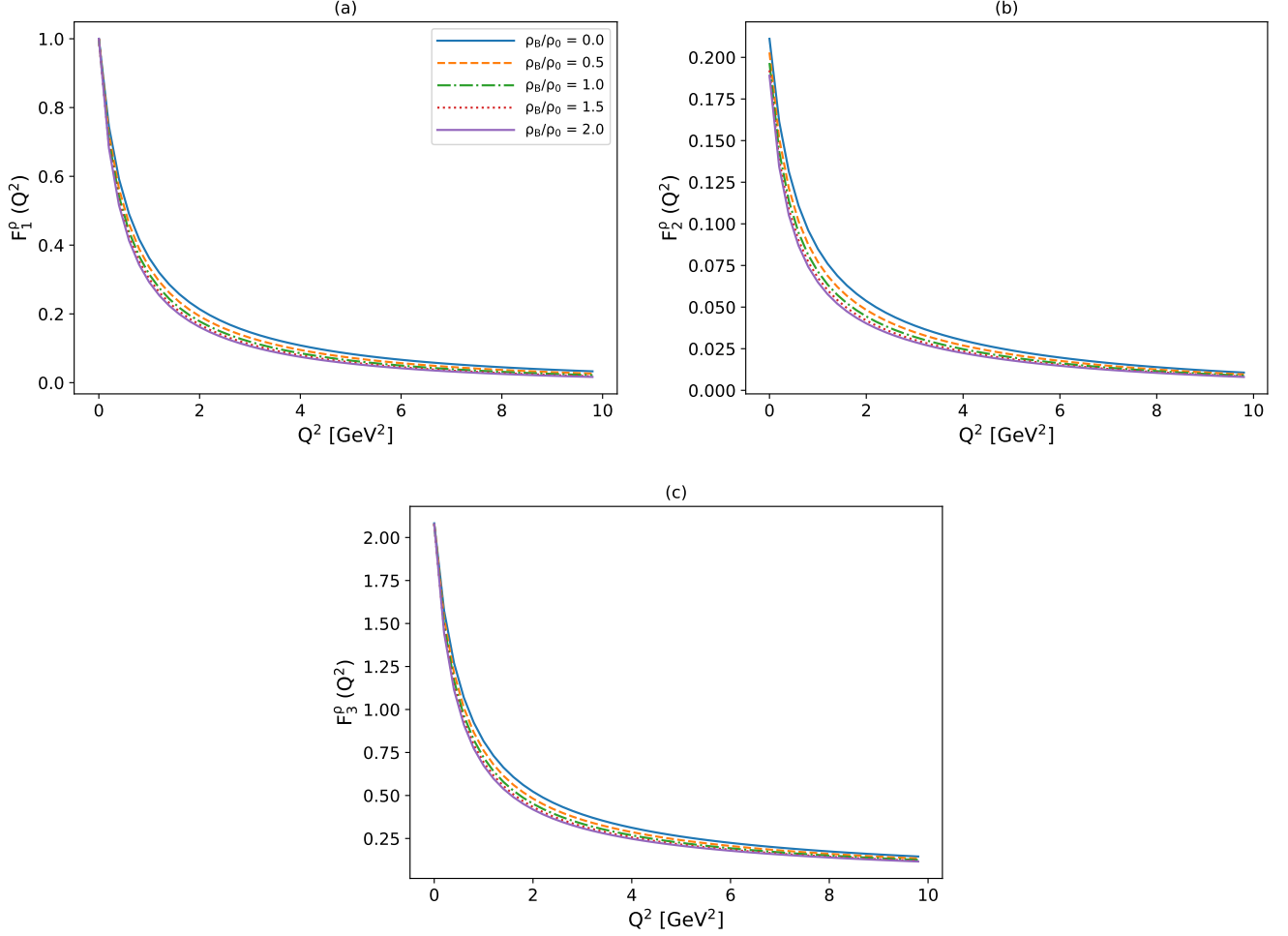


FIG. 5. Results of the ρ^+ meson EMFFs for different densities (a) $F_1^{\rho}(Q^2)$, (b) $F_2^{\rho}(Q^2)$, and (c) $F_3^{\rho}(Q^2)$ for different nuclear matter densities as a function of Q^2 .

for $F_2^{\rho}(Q^2)$ decrease as the nuclear matter density and Q^2 increase. The decrease of $F_2^{\rho}(Q^2)$ is more pronounced at higher nuclear matter densities. We also find that in free space, our results are consistent with those reported in Ref. [54].

Results for the $F_3^{\rho}(Q^2)$ for different nuclear matter densities as a function of Q^2 are given in Fig. 5(c). Similar to the results of $F_1^{\rho}(Q^2)$ and $F_2^{\rho}(Q^2)$, we find that the $F_3^{\rho}(Q^2)$ decreases as the nuclear matter density ρ_B/ρ_0 and Q^2 increase. It is more significant at higher ρ_B/ρ_0 . Again, our results of $F_3^{\rho}(Q^2)$ in free space are consistent with those obtained in Ref. [54]. It is worth noting that in free space, $F_3^{\rho}(Q^2 = 0)$ equals the magnetic moment of the ρ meson. The decrease of $F_3^{\rho}(Q^2 = 0)$ at $\rho_B/\rho_0 = 1.0$ is approximately 0.15% in comparison to that for free space ($\rho_B/\rho_0 = 0.0$), which is insignificant reduction. At higher nuclear matter density, $\rho_B/\rho_0 = 2.0$, we find a reduction of the $F_3^{\rho}(Q^2 = 0)$ by approximately 0.24% in comparison to that in free space, and again, insignificant.

We are now in a position to present the in-medium ρ^+ meson EMFFs: the charge form factor $G_C^{\rho}(Q^2)$ in units of the positron charge e , the magnetic form factor $G_M^{\rho}(Q^2)$ in units of $e/(2m_{\rho})$, and the quadrupole form factor $G_Q^{\rho}(Q^2)$ in units of e/m_{ρ}^2 , both in free space and in nuclear matter. Results for the ρ^+ meson charge form factor for different nuclear matter densities as a function of Q^2 are illustrated in Fig. 6(a). We find that the values of $G_C^{\rho}(Q^2)$ in free space are positive up to $Q^2 \leq 3.2$ GeV². At $Q^2 \geq 3.4$ GeV², the values of $G_C^{\rho}(Q^2)$ become negative. At $Q^2 = 0$, $G_C^{\rho}(Q^2)$ satisfies the charge normalization (charge conservation), namely, $G_C^{\rho}(0) = 1.0$. This occurs not only in free space but also in a nuclear medium. At $\rho_B/\rho_0 = 1.0$, the positive values of $G_C^{\rho}(Q^2)$ slightly move up to $Q^2 \leq 2.6$ GeV², and for $Q^2 \geq 2.8$ GeV², the values of $G_C^{\rho}(Q^2)$ become negative, which starts smaller Q^2 value than that for free space. At higher nuclear matter density $\rho_B/\rho_0 = 2.0$, the values of $G_C^{\rho}(Q^2)$ become positive for $Q^2 \leq 2.2$ GeV², while

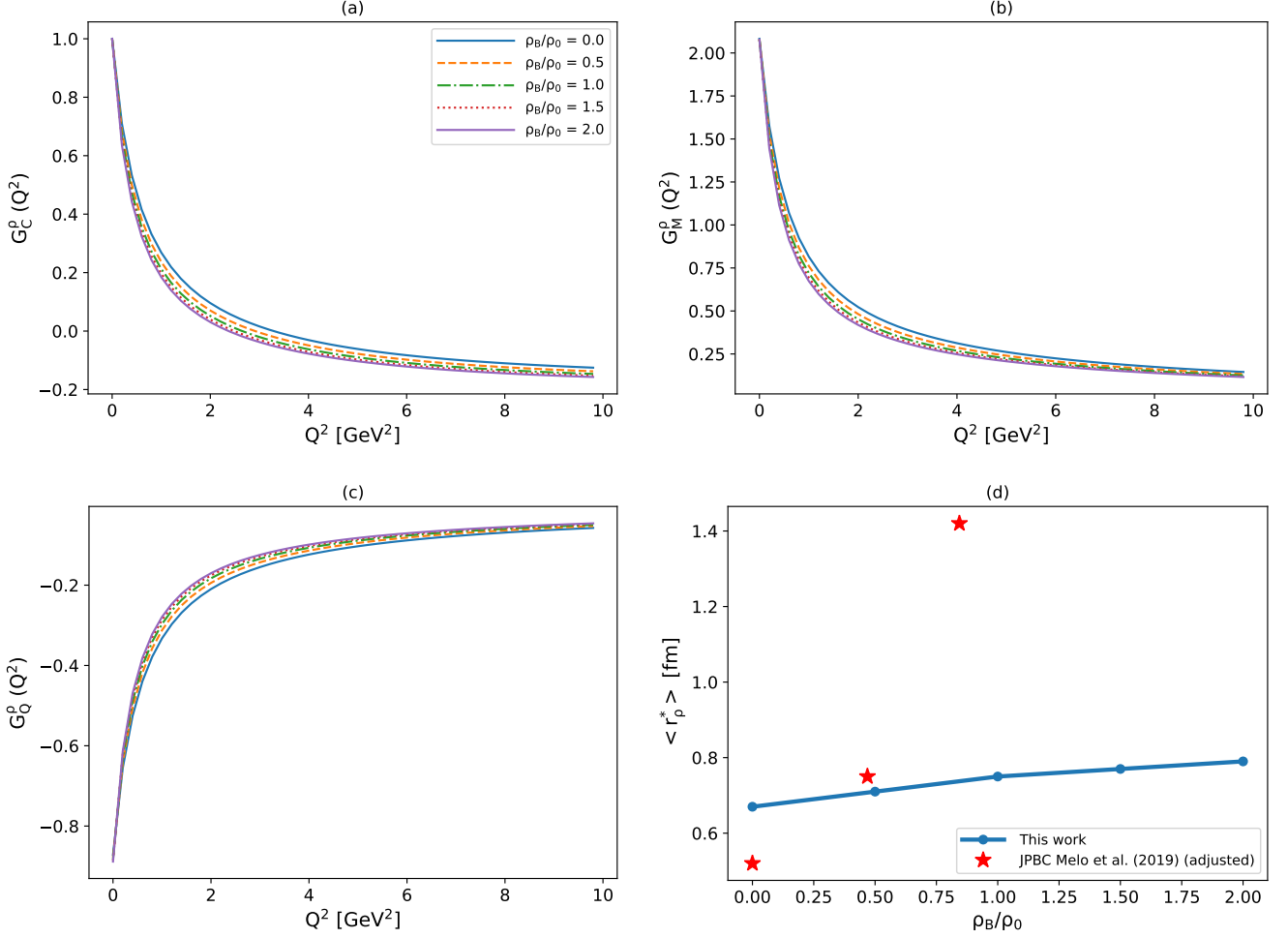


FIG. 6. Results for the ρ^+ meson EM properties, (a) the charge form factors, (b) magnetic form factors, (c) quadrupole form factors, and (d) charge radius, $\langle r_\rho^* \rangle \equiv \langle r_C^{*2} \rangle^{1/2}$, as a function of ρ_B/ρ_0 . See also the caption of Fig. 2 for the note on the asterisk (red) data.

$G_C^{*\rho}(Q^2)$ becomes negative at $Q^2 \geq 2.4 \text{ GeV}^2$. Our result of $G_C^\rho(Q^2)$ in free space is consistent with those reported in Ref. [54].

Let us now discuss our results for the $G_C^{*\rho}(Q^2)$ in the nuclear medium. Our results are consistent with those obtained in Ref. [52]. However, the differences are in the Q^2 values for crossing negative-positive values and the magnitudes. The results reported in Ref. [52] indicated that $G_C^{*\rho}(Q^2)$ in nuclear matter is softer compared to our results. This is indicated by the onset of the negative values in $G_C^{*\rho}(Q^2)$ occurring at a lower Q^2 , i.e., at a smaller Q^2 value.

Next, in Fig. 6(b), we show our predictions for ρ^+ meson magnetic moment form factors, $G_M^{*\rho}(Q^2)$ for different values of ρ_B/ρ_0 and Q^2 . We find that the $G_M^{*\rho}(Q^2)$ decreases as the ρ_B/ρ_0 and Q^2 increase. This behavior of $G_M^{*\rho}(Q^2)$ is consistent with the trend reported in Ref. [52], although the magnitudes differ. Note that the $G_M^{*\rho}(Q^2)$ at $Q^2 = 0$ equals to the ρ^+ meson magnetic moment, μ_ρ^* . In this work, we follow the formula of Ref. [13] in free space, where $\mu_\rho = G_M(0) \frac{M_N}{m_\rho}$. In the nuclear medium, the expression of μ_ρ is defined as $\mu_\rho^* = G_M^*(0) \frac{M_N^*}{m_\rho^*}$. The values of m_ρ^* and M_N^* for various nuclear matter densities are given in Table I. We find that the value of $G_M^\rho(Q^2)$ in free space at $Q^2 = 0$ is 2.082, in agreement with the value obtained in Ref. [54], while at $\rho_B/\rho_0 = 1.0$, we obtain $G_M^{*\rho}(0) = 2.079$, which is very similar magnitude to that in free space. At higher density $\rho_B/\rho_0 = 2.0$, the value of $G_M^{*\rho}(0)$ is 2.077. The value of $G_M^{*\rho}(0)$ is 2.081 at $\rho_B/\rho_0 = 0.5$, which is smaller than the result obtained in Ref. [52], i.e., $G_M^{*\rho}(0) = 2.18$ at $\rho_B/\rho_0 = 0.5$.

Results for the quadrupole moment form factors of ρ^+ meson $G_Q^{*\rho}(Q^2)$ for different nuclear matter densities as a

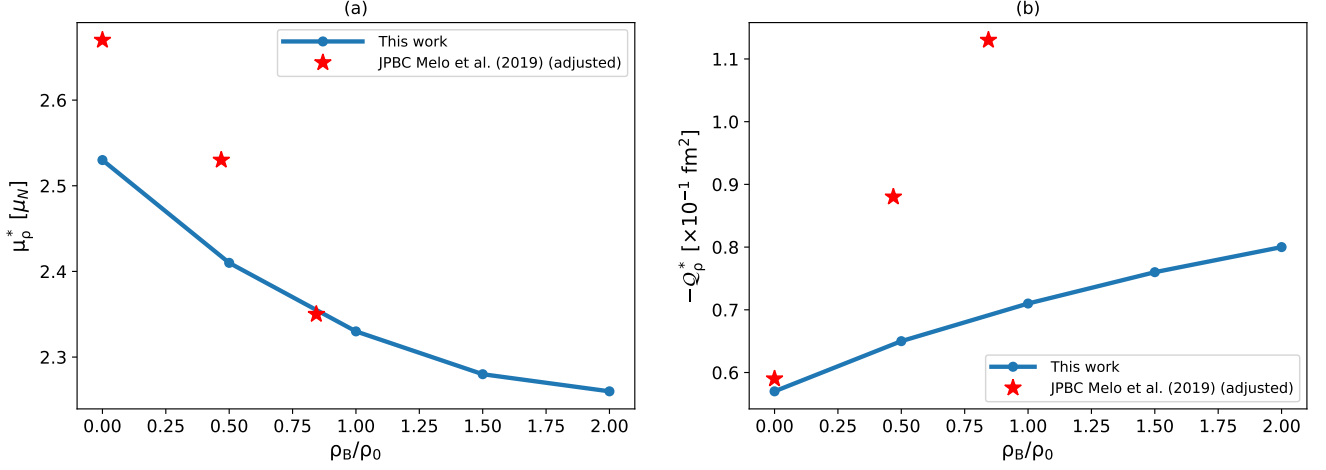


FIG. 7. Results for (a) magnetic moment, and (b) quadrupole moment of ρ^+ meson as a function of ρ_B/ρ_0 . See also the caption of Fig. 2 for the note on the filled asterisk (red) data.

function of Q^2 are illustrated in Fig. 6(c). We find that the $G_Q^{*\rho}(Q^2)$ increases as the nuclear matter density and Q^2 increase. In free space, our result is consistent with that obtained in Ref. [13, 54]. Also, we obtain the same values of $G_Q^{*\rho}(Q^2)$ at $Q^2 = 0$ with those reported in Refs. [13, 54], i.e., $G_Q^{*\rho}(0) = -0.87$ in free space. However, this value is rather different from that obtained in Ref. [52] in free space and also the value in nuclear matter. The difference is not only found in the values of $G_Q^{*\rho}(0)$, but also in the Q^2 dependence of $G_Q^{*\rho}(Q^2)$ for specific nuclear matter densities as shown in the lower-left panel of Fig. 5 in Ref. [52], where there is zero crossings in $G_Q^{*\rho}(Q^2)$ for $\rho_B/\rho_0 = 0.00, 0.25$, and 0.50 at low Q^2 . Such behavior is not found in our results for the $G_Q^{*\rho}(Q^2)$, as clearly shown in Fig. 6(c). We find that the values of the $G_Q^{*\rho}(0)$ for $\rho_B/\rho_0 = 0.5, 1.0, 1.5$, and 2.0 are $-0.878, -0.883, -0.886$, and -0.888 , respectively.

In Fig. 6 (d), we show the results for the ρ^+ meson in-medium charge radius $\langle r_\rho^* \rangle \equiv \langle r_C^{*2} \rangle^{1/2}$ as a function of ρ_B/ρ_0 . We find that the charge radius increases as the nuclear matter density increases. In free space, it is consistent with the value obtained in Ref. [54], i.e., $\langle r_\rho \rangle = 0.67$ fm. However, this is rather different from that obtained in Ref. [52], i.e., $\langle r_\rho \rangle = 0.52$ fm, as also clearly indicated in Fig. 6(d). Furthermore, our result in free space differs significantly from that of Ref. [13], where it was reported $\langle r_\rho \rangle = 0.82$ fm. This discrepancy arises from the absence of pion loop contributions in the present work. Figure 6(d) also shows a comparison of our charge radius with that of Ref. [52]. The charge radius of Ref. [52] at $\rho_B/\rho_0 = 0.50$ (red filled asterisks) are close to our results (blue solid line). However, the results for $\langle r_\rho^* \rangle$ are quite different from our results, as one can clearly see at $\rho_B/\rho_0 = (0.0, \text{ and } 0.90)$. Note that, as already explained earlier, here we emphasize again that the $\rho_B/\rho_0 = 0.9$ corresponds to 0.84375 in the present study, as indicated in Fig. 6(d). For convenience, the values of the charge radius, quadrupole moment, and magnetic moment of the ρ meson at various densities are listed in Table I.

Finally, we show the results of the ρ^+ meson magnetic and quadrupole moments for different nuclear matter densities, respectively, compared with those reported in Ref. [52], as depicted in Fig. 7(a)-(b). In Fig. 7(a), we show the result for the magnetic moment. We find that the ρ^+ meson magnetic moment decreases as the nuclear matter density increases. In addition, we find that our results for the magnetic moment are rather close to those obtained in Ref. [52]. The behavior of μ_p^* exhibits a similar trend to our prediction, as in Fig. 7(a), where the ρ^+ meson magnetic moment decreases with increasing nuclear matter density. We find $\mu_p^* = 2.41\mu_N$ at $\rho_B/\rho_0 = 0.5$, whereas Ref. [52] reports $\mu_p^* = 2.53\mu_N$ at the same density.

In Fig. 7(b), we show the results for the quadrupole moment of the ρ^+ meson as a function of the nuclear matter densities. We find that the Q_p^* increases as the nuclear matter density increases. Again, a similar trend is reported in Ref. [52], indicating the Q_p^* increases as the ρ_B/ρ_0 increases. At $\rho_B/\rho_0 = 0.0$ (free space) they obtained $Q_p^* = -0.059$ fm², which is close to our free space value, $Q_p^* = -0.057$ fm². However, at $\rho_B/\rho_0 = 0.5$ in their units with $\rho_0 = 0.15$ fm⁻³, namely 0.46785 in the present units, the values of Q_p^* is rather different. At this point, our calculation yields $Q_p^* = -0.065$ fm², whereas the value they obtained is $Q_p^* = -0.088$ fm², which is smaller than ours. As ρ_B/ρ_0 increases, the difference becomes more significant.

VII. SUMMARY AND CONCLUSION

To summarize, we have investigated the in-medium modifications of the electromagnetic properties (form factors and charge radius) of the ρ meson within the framework of the Nambu–Jona-Lasino (NJL) model, utilizing the Schwinger proper-time regularization scheme to simulate quark confinement. The effect of the nuclear medium is consistently studied in the NJL model at the quark level, where the chiral symmetry breaking and the partial restoration can be described in the NJL model *via* the quark condensate appearing in the model. Thus, we systematically investigate the properties and structure of ρ meson in free space and in symmetric nuclear matter, such as the effective mass, in-medium dynamical quark mass, in-medium ρ -quark coupling constant, and ρ meson electromagnetic properties, namely charge form factor, charge radius, magnetic moment, and quadrupole moment.

As a result, we have found that the ρ meson effective mass decreases as the nuclear matter density increases. This is consistent with that obtained in Ref. [52], although the magnitude is different. We find the ρ meson mass reduction at $\rho_B/\rho_0 = 1.0$ relative to that in free space is about 10%, which is consistent with that obtained in the QCD sum rule (QCDSR) of Ref. [43], and a very recent analysis in the inverse QCD sum rule (IQCDSR) of Ref. [45], giving about (10-20)%. However, the reduction of the m_ρ^* of Ref. [52] is rather different from that obtained in the present work, as clearly shown in Fig. 2(a), where in the former, the in-medium ρ mass was calculated in the quark-meson coupling (QMC) model using a rather larger free space light quark mass value compared to that used in the standard QMC model.

A similar trend is found in the in-medium dynamical quark mass, where the in-medium dynamical quark mass decreases as the nuclear matter density increases, as clearly illustrated in Fig. 2(b). The in-medium constituent quark mass results reported in Ref. [52] exhibit a similar trend to our predictions, showing a decrease with increasing nuclear matter density. However, their results show a more rapid decrease in the in-medium constituent quark mass calculated by the QMC model with a large free space light quark mass value.

We predict the in-medium ρ -meson-quark coupling constant in the nuclear medium. As expected, the ρ -meson-quark coupling constant decreases as the nuclear matter density increases. We also find that the reduction of the ρ -meson-quark coupling constant at $\rho_B/\rho_0 = 1.0$ relative to that in free space is approximately 7%.

We have presented that the Bethe-Salpeter equation (BSE) calculated dressed quark electromagnetic form factors for different densities and Q^2 . We have found that $F_{1D}^*(Q^2)$ increases up to $Q^2 \simeq 2 \text{ GeV}^2$ and then continues to decrease up to higher Q^2 . However, $F_{1D}^*(Q^2)$ does not go to zero. It behaves as $F_{1D}^*(Q^2) = e_d$ at $Q^2 \rightarrow \infty$, which is consistent with the expectation of QCD in the asymptotic regime.

We have also shown the results for the $F_{1U}^*(Q^2)$, which exhibits the decrease of $F_{1U}^*(Q^2)$ up to $Q^2 \simeq 2 \text{ GeV}^2$ and then continues to increase as the Q^2 increases. However, it decreases as the nuclear matter density increases. It is worth noting that the opposite of Q^2 dependent behavior to that of $F_{1D}^*(Q^2)$, is due to the opposite sign of the charge. At $Q^2 \rightarrow \infty$, $F_{1U}^*(Q^2) \simeq e_u$, which is consistent with the QCD expectation in the asymptotic regime.

For the results of the vector body form factors, we have found that, $f_1^{*V}(Q^2)$, $f_2^{*V}(Q^2)$, and $f_3^{*V}(Q^2)$ decrease as the nuclear matter density and Q^2 increase. This behavior is followed by the ρ^+ meson electromagnetic form factors, $F_1^{\rho^*}(Q^2)$, $F_2^{\rho^*}(Q^2)$, and $F_3^{\rho^*}(Q^2)$, giving a decrease of these ρ meson form factors as the nuclear matter density and Q^2 increase, as illustrated in Fig. 5(a)-(c).

In addition, we have predicted the in-medium ρ^+ meson charge radius, that increases as the nuclear matter density increases. Our prediction for the in-medium charge radius is consistent with that obtained in Ref. [52], although different in magnitude, as indicated in Fig. 6(d).

Finally, we have predicted the ρ^+ meson magnetic and quadrupole moments in symmetric nuclear matter. We have found that the μ_ρ^* decreases as the nuclear matter density increases. The trends of our results are consistent with those obtained in Ref. [52], but different in magnitude. For the quadrupole moment, we have found that the Q_ρ^* increases as the nuclear matter density increases. Our predictions are consistent with those obtained in Ref. [52], however, again, different in magnitude, in particular at higher nuclear matter densities.

Overall, the predictions presented in this work are potentially testable by the future experiments, such as JPARC E16 [60], and CLAS at JLAB [39, 40], as well as lattice QCD [61–63]. For future work, we plan to apply the present approach to investigate the electromagnetic form factors of other spin-1 mesons in a nuclear medium, as well as pseudoscalar D and B mesons with heavy c and b quark contents, where such studies may require significant challenges, since heavy quark symmetry differs fundamentally from the light quark symmetry. Furthermore, we hope that the present study can provide useful guidance for lattice QCD in computing the electromagnetic form factors of the ρ meson in free space as well as in a nuclear medium.

ACKNOWLEDGEMENTS

This work was supported by the PUTI Q1 Research Grant from the University of Indonesia (UI) under contract No. NKB 442/UN2.RST/HKP.05.00/2024. K.T. was supported by Conselho Nacional de Desenvolvimento Científico e Tecnológico (CNPq, Brazil), Processes No. 304199/2022-2, and FAPESP Process No. 2023/07313-6, and his work was also part of the projects, Instituto Nacional de Ciência e Tecnologia - Nuclear Physics and Applications (INCT-FNA), Brazil, Process No. 464898/2014-5.

-
- [1] B. L. Ioffe, QCD at low energies, Prog. Part. Nucl. Phys. 56 (2006) 232–277. [arXiv:hep-ph/0502148](#), [doi:10.1016/j.pnpnp.2005.05.001](#).
 - [2] A. Deur, S. J. Brodsky, G. F. de Teramond, The QCD Running Coupling, Nucl. Phys. 90 (2016) 1. [arXiv:1604.08082](#), [doi:10.1016/j.pnpnp.2016.04.003](#).
 - [3] Y. V. Kovchegov, H. Sun, Z. Tu, Novel cross section ratios as possible signals of saturation in ultraperipheral collisions, Phys. Rev. D 109 (9) (2024) 094028. [arXiv:2311.12208](#), [doi:10.1103/PhysRevD.109.094028](#).
 - [4] F. Gross, et al., 50 Years of Quantum Chromodynamics, Eur. Phys. J. C 83 (2023) 1125. [arXiv:2212.11107](#), [doi:10.1140/epjc/s10052-023-11949-2](#).
 - [5] V. V. Braguta, A. I. Onishchenko, rho meson form-factors and QCD sum rules, Phys. Rev. D 70 (2004) 033001. [arXiv:hep-ph/0403258](#), [doi:10.1103/PhysRevD.70.033001](#).
 - [6] F. Cardarelli, I. L. Grach, I. M. Narodetsky, G. Salme, S. Simula, Electromagnetic form-factors of the rho meson in a light front constituent quark model, Phys. Lett. B 349 (1995) 393–399. [arXiv:hep-ph/9502360](#), [doi:10.1016/0370-2693\(95\)00230-I](#).
 - [7] J. P. B. C. de Melo, T. Frederico, Light-Front projection of spin-1 electromagnetic current and zero-modes, Phys. Lett. B 708 (2012) 87–92. [arXiv:1202.0734](#), [doi:10.1016/j.physletb.2012.01.021](#).
 - [8] W. Jaus, Consistent treatment of spin 1 mesons in the light front quark model, Phys. Rev. D 67 (2003) 094010. [arXiv:hep-ph/0212098](#), [doi:10.1103/PhysRevD.67.094010](#).
 - [9] T. M. Aliev, A. Ozpineci, M. Savci, Magnetic and quadrupole moments of light spin-1 mesons in light cone QCD sum rules, Phys. Lett. B 678 (2009) 470–476. [arXiv:0902.4627](#), [doi:10.1016/j.physletb.2009.06.073](#).
 - [10] M. S. Bhagwat, P. Maris, Vector meson form factors and their quark-mass dependence, Phys. Rev. C 77 (2008) 025203. [arXiv:nuc1-th/0612069](#), [doi:10.1103/PhysRevC.77.025203](#).
 - [11] Y.-Z. Xu, The electromagnetic form factors of heavy-light pseudo-scalar and vector mesons, JHEP 07 (2024) 118. [arXiv:2402.06141](#), [doi:10.1007/JHEP07\(2024\)118](#).
 - [12] C. Shi, J. Li, P.-L. Yin, W. Jia, Unpolarized generalized parton distributions of light and heavy vector mesons, Phys. Rev. D 107 (7) (2023) 074009. [arXiv:2302.02388](#), [doi:10.1103/PhysRevD.107.074009](#).
 - [13] M. E. Carrillo-Serrano, W. Bentz, I. C. Cloët, A. W. Thomas, ρ meson form factors in a confining Nambu–Jona-Lasinio model, Phys. Rev. C 92 (1) (2015) 015212. [arXiv:1504.08119](#), [doi:10.1103/PhysRevC.92.015212](#).
 - [14] W. Qian, S. Jia, Y. Li, J. P. Vary, Light mesons within the basis light-front quantization framework, Phys. Rev. C 102 (5) (2020) 055207. [arXiv:2005.13806](#), [doi:10.1103/PhysRevC.102.055207](#).
 - [15] H. Habermann, Model-independent form-factor constraints for electromagnetic spin-1 currents, Phys. Rev. D 100 (3) (2019) 036008. [arXiv:1905.06299](#), [doi:10.1103/PhysRevD.100.036008](#).
 - [16] A. F. Krutov, R. G. Polezhaev, V. E. Troitsky, Magnetic moment of the ρ meson in instant-form relativistic quantum mechanics, Phys. Rev. D 97 (3) (2018) 033007. [arXiv:1801.01458](#), [doi:10.1103/PhysRevD.97.033007](#).
 - [17] W.-Y. Liu, E. Shuryak, I. Zahed, Hadronic structure on the light front. VIII. Light scalar and vector mesons, Phys. Rev. D 109 (7) (2024) 074029. [arXiv:2307.16302](#), [doi:10.1103/PhysRevD.109.074029](#).
 - [18] S. Kumano, Q.-T. Song, Equation-of-motion and Lorentz-invariance relations for tensor-polarized parton distribution functions of spin-1 hadrons, Phys. Lett. B 826 (2022) 136908. [arXiv:2112.13218](#), [doi:10.1016/j.physletb.2022.136908](#).
 - [19] F. Gao, L. Chang, Y.-X. Liu, C. D. Roberts, S. M. Schmidt, Parton distribution amplitudes of light vector mesons, Phys. Rev. D 90 (1) (2014) 014011. [arXiv:1405.0289](#), [doi:10.1103/PhysRevD.90.014011](#).
 - [20] P. Ball, V. M. Braun, A. Lenz, Twist-4 distribution amplitudes of the K^* and phi mesons in QCD, JHEP 08 (2007) 090. [arXiv:0707.1201](#), [doi:10.1088/1126-6708/2007/08/090](#).
 - [21] A. J. Arifi, P. T. P. Hutaeruk, K. Tsushima, In-medium properties of the light and heavy-light mesons in a light-front quark model, Phys. Rev. D 107 (11) (2023) 114010. [arXiv:2302.12382](#), [doi:10.1103/PhysRevD.107.114010](#).
 - [22] S. Kumano, Q.-T. Song, Transverse-momentum-dependent parton distribution functions up to twist 4 for spin-1 hadrons, Phys. Rev. D 103 (1) (2021) 014025. [arXiv:2011.08583](#), [doi:10.1103/PhysRevD.103.014025](#).
 - [23] Y. Ninomiya, W. Bentz, I. C. Cloët, Transverse-momentum-dependent quark distribution functions of spin-one targets: Formalism and covariant calculations, Phys. Rev. C 96 (4) (2017) 045206. [arXiv:1707.03787](#), [doi:10.1103/PhysRevC.96.045206](#).
 - [24] B.-D. Sun, Y.-B. Dong, Gravitational form factors of ρ meson with a light-cone constituent quark model, Phys. Rev. D 101 (9) (2020) 096008. [arXiv:2002.02648](#), [doi:10.1103/PhysRevD.101.096008](#).

- [25] J.-Y. Kim, B.-D. Sun, D. Fu, H.-C. Kim, Mechanical structure of a spin-1 particle, *Phys. Rev. D* 107 (5) (2023) 054007. [arXiv:2208.01240](#), [doi:10.1103/PhysRevD.107.054007](#).
- [26] B. Sun, Y. Dong, Generalized parton distribution functions of ρ meson, *SciPost Phys. Proc.* 3 (2020) 014. [doi:10.21468/SciPostPhysProc.3.014](#).
- [27] D. F. Geesaman, K. Saito, A. W. Thomas, The nuclear EMC effect, *Ann. Rev. Nucl. Part. Sci.* 45 (1995) 337–390. [doi:10.1146/annurev.ns.45.120195.002005](#).
- [28] J. J. Aubert, et al., The ratio of the nucleon structure functions F_{2n} for iron and deuterium, *Phys. Lett. B* 123 (1983) 275–278. [doi:10.1016/0370-2693\(83\)90437-9](#).
- [29] R. S. Hayano, T. Hatsuda, Hadron properties in the nuclear medium, *Rev. Mod. Phys.* 82 (2010) 2949. [arXiv:0812.1702](#), [doi:10.1103/RevModPhys.82.2949](#).
- [30] O. Hen, G. A. Miller, E. Piasetzky, L. B. Weinstein, Nucleon-Nucleon Correlations, Short-lived Excitations, and the Quarks Within, *Rev. Mod. Phys.* 89 (4) (2017) 045002. [arXiv:1611.09748](#), [doi:10.1103/RevModPhys.89.045002](#).
- [31] G. Gifari, P. T. P. Hutaaruk, T. Mart, Nuclear medium meson structures from the Schwinger proper-time Nambu–Jona-Lasinio model, *Phys. Rev. D* 110 (1) (2024) 014043. [arXiv:2402.19048](#), [doi:10.1103/PhysRevD.110.014043](#).
- [32] P. T. P. Hutaaruk, Y. Oh, K. Tsushima, Electroweak properties of pions in a nuclear medium, *Phys. Rev. C* 99 (1) (2019) 015202. [arXiv:1810.08874](#), [doi:10.1103/PhysRevC.99.015202](#).
- [33] P. T. P. Hutaaruk, I. C. Cloet, A. W. Thomas, Flavor dependence of the pion and kaon form factors and parton distribution functions, *Phys. Rev. C* 94 (3) (2016) 035201. [arXiv:1604.02853](#), [doi:10.1103/PhysRevC.94.035201](#).
- [34] P. T. P. Hutaaruk, S.-i. Nam, Gluon and valence quark distributions for the pion and kaon in nuclear matter, *Phys. Rev. D* 105 (3) (2022) 034021. [arXiv:2112.05435](#), [doi:10.1103/PhysRevD.105.034021](#).
- [35] G. R. Farrar, D. R. Jackson, The Pion Form-Factor, *Phys. Rev. Lett.* 43 (1979) 246. [doi:10.1103/PhysRevLett.43.246](#).
- [36] V. Bernard, U. G. Meissner, Electromagnetic Structure of the Pion and the Kaon, *Phys. Rev. Lett.* 61 (1988) 2296, [Erratum: *Phys. Rev. Lett.* 61, 2973 (1988)]. [doi:10.1103/PhysRevLett.61.2296](#).
- [37] P. T. P. Hutaaruk, J. J. Cobos-Martínez, Y. Oh, K. Tsushima, Valence-quark distributions of pions and kaons in a nuclear medium, *Phys. Rev. D* 100 (9) (2019) 094011. [arXiv:1908.02406](#), [doi:10.1103/PhysRevD.100.094011](#).
- [38] W. Cassing, W. Ehehalt, C. M. Ko, Dilepton production at SPS energies, *Phys. Lett. B* 363 (1995) 35–40. [arXiv:hep-ph/9508233](#), [doi:10.1016/0370-2693\(95\)01214-B](#).
- [39] M. H. Wood, et al., Light Vector Mesons in the Nuclear Medium, *Phys. Rev. C* 78 (2008) 015201. [arXiv:0803.0492](#), [doi:10.1103/PhysRevC.78.015201](#).
- [40] R. Nasseripour, et al., Search for medium modification of the rho meson, *Phys. Rev. Lett.* 99 (2007) 262302. [arXiv:0707.2324](#), [doi:10.1103/PhysRevLett.99.262302](#).
- [41] M. Naruki, et al., Experimental signature of the medium modification for rho and omega mesons in 12-GeV p + A reactions, *Phys. Rev. Lett.* 96 (2006) 092301. [arXiv:nucl-ex/0504016](#), [doi:10.1103/PhysRevLett.96.092301](#).
- [42] K. Ozawa, et al., Observation of rho / omega meson modification in nuclear matter, *Phys. Rev. Lett.* 86 (2001) 5019–5022. [arXiv:nucl-ex/0011013](#), [doi:10.1103/PhysRevLett.86.5019](#).
- [43] T. Hatsuda, S. H. Lee, QCD sum rules for vector mesons in the nuclear medium, *Phys. Rev. C* 46 (1) (1992) R34. [doi:10.1103/PhysRevC.46.R34](#).
- [44] M. Asakawa, C. M. Ko, Medium effects on the rho meson, *Phys. Rev. C* 48 (2) (1993) R526. [doi:10.1103/PhysRevC.48.R526](#).
- [45] H. Mutuk, Reappraisal of the rho meson in nuclear matter by the inverse QCD sum rules method, *Phys. Rev. D* 111 (9) (2025) 094029. [arXiv:2503.10343](#), [doi:10.1103/PhysRevD.111.094029](#).
- [46] D. Cabrera, E. Oset, M. J. Vicente Vacas, Chiral approach to the rho meson in nuclear matter, *Nucl. Phys. A* 705 (2002) 90–118. [arXiv:nucl-th/0011037](#), [doi:10.1016/S0375-9474\(02\)00612-7](#).
- [47] V. Bernard, U. G. Meissner, Properties of Vector and Axial Vector Mesons from a Generalized Nambu–Jona-Lasinio Model, *Nucl. Phys. A* 489 (1988) 647–670. [doi:10.1016/0375-9474\(88\)90114-5](#).
- [48] C. M. Ko, Rho meson spectral function in dense matter, *Phys. Rept.* 242 (1994) 453–461. [doi:10.1016/0370-1573\(94\)90178-3](#).
- [49] G. Chanfray, P. Schuck, rho meson mass spectrum in dense matter, *Nucl. Phys. A* 545 (1992) 271C–276C. [doi:10.1016/0375-9474\(92\)90467-X](#).
- [50] R. Rapp, G. Chanfray, J. Wambach, Rho meson propagation and dilepton enhancement in hot hadronic matter, *Nucl. Phys. A* 617 (1997) 472–495. [arXiv:hep-ph/9702210](#), [doi:10.1016/S0375-9474\(97\)00137-1](#).
- [51] L. A. Kondratyuk, A. Sibirtsev, W. Cassing, Y. S. Golubeva, M. Effenberger, Rho meson properties at finite nuclear density, *Phys. Rev. C* 58 (1998) 1078–1085. [arXiv:nucl-th/9801055](#), [doi:10.1103/PhysRevC.58.1078](#).
- [52] J. P. B. C. de Melo, K. Tsushima, ρ -meson properties in medium, *Phys. Lett. B* 788 (2019) 137–146. [arXiv:1802.06096](#), [doi:10.1016/j.physletb.2018.10.059](#).
- [53] W. Bentz, A. W. Thomas, The Stability of nuclear matter in the Nambu–Jona-Lasinio model, *Nucl. Phys. A* 696 (2001) 138–172. [arXiv:nucl-th/0105022](#), [doi:10.1016/S0375-9474\(01\)01119-8](#).
- [54] I. C. Cloët, W. Bentz, A. W. Thomas, Role of diquark correlations and the pion cloud in nucleon elastic form factors, *Phys. Rev. C* 90 (2014) 045202. [arXiv:1405.5542](#), [doi:10.1103/PhysRevC.90.045202](#).
- [55] S. P. Klevansky, The Nambu–Jona-Lasinio model of quantum chromodynamics, *Rev. Mod. Phys.* 64 (1992) 649–708. [doi:10.1103/RevModPhys.64.649](#).
- [56] N. Ishii, W. Bentz, K. Yazaki, Solution of the relativistic three quark Faddeev equation in the Nambu–Jona-Lasinio (NJL) model, *Phys. Lett. B* 318 (1993) 26–31. [doi:10.1016/0370-2693\(93\)91778-L](#).

- [57] G. Krein, A. W. Thomas, K. Tsushima, Fock terms in the quark meson coupling model, Nucl. Phys. A 650 (1999) 313–325. [arXiv:nuc1-th/9810023](#), [doi:10.1016/S0375-9474\(99\)00117-7](#).
- [58] C. M. Shakin, W.-D. Sun, Properties of the rho meson in nuclear matter, Phys. Rev. C 49 (1994) 1185–1189. [doi:10.1103/PhysRevC.49.1185](#).
- [59] Z.-Y. Zhu, A. Li, J.-N. Hu, H. Shen, Quark mean-field model for nuclear matter with or without bag, Phys. Rev. C 99 (2) (2019) 025804. [arXiv:1805.04678](#), [doi:10.1103/PhysRevC.99.025804](#).
- [60] K. Aoki, Study of in-medium mass modification at J-PARC, in: 10th Workshop on Particle Correlations and Femtoscopy, 2015. [arXiv:1502.00703](#).
- [61] J. N. Hedditch, W. Kamleh, B. G. Lasscock, D. B. Leinweber, A. G. Williams, J. M. Zanotti, Pseudoscalar and vector meson form-factors from lattice QCD, Phys. Rev. D 75 (2007) 094504. [arXiv:hep-lat/0703014](#), [doi:10.1103/PhysRevD.75.094504](#).
- [62] B. Owen, W. Kamleh, D. Leinweber, B. Menadue, S. Mahbub, Light Meson Form Factors at near Physical Masses, Phys. Rev. D 91 (7) (2015) 074503. [arXiv:1501.02561](#), [doi:10.1103/PhysRevD.91.074503](#).
- [63] Z. Wang, D. B. Leinweber, C. Liu, L. Liu, P. Sun, A. W. Thomas, J.-j. Wu, H. Xing, K. Yu, Spectral parameters of the ρ resonance from lattice QCD, JHEP 08 (2025) 064. [arXiv:2502.03700](#), [doi:10.1007/JHEP08\(2025\)064](#).